



HAL
open science

Climatic reconstruction for the Younger Dryas/Early Holocene transition and the Little Ice Age based on paleo-extents of Argentière glacier (French Alps)

Marie Protin, Irene Schimmelpfennig, Jean-louis Mugnier, Ludovic Ravel, Melaine Le Roy, Philip Deline, Vincent Favier, Jean-François Buoncristiani, Team Aster, Didier Boulès, et al.

► To cite this version:

Marie Protin, Irene Schimmelpfennig, Jean-louis Mugnier, Ludovic Ravel, Melaine Le Roy, et al.. Climatic reconstruction for the Younger Dryas/Early Holocene transition and the Little Ice Age based on paleo-extents of Argentière glacier (French Alps). *Quaternary Science Reviews*, 2019, 221, pp.105863. 10.1016/j.quascirev.2019.105863. hal-03102778

HAL Id: hal-03102778

<https://hal.science/hal-03102778v1>

Submitted on 7 Jan 2021

HAL is a multi-disciplinary open access archive for the deposit and dissemination of scientific research documents, whether they are published or not. The documents may come from teaching and research institutions in France or abroad, or from public or private research centers.

L'archive ouverte pluridisciplinaire **HAL**, est destinée au dépôt et à la diffusion de documents scientifiques de niveau recherche, publiés ou non, émanant des établissements d'enseignement et de recherche français ou étrangers, des laboratoires publics ou privés.

1 **Climatic reconstruction for the Younger Dryas/Early Holocene**
2 **transition and the Little Ice Age based on paleo-extents of**
3 **Argentière glacier (French Alps)**

4

5 Marie Protin^a, Irene Schimmelpfennig^a, Jean-Louis Mugnier^b, Ludovic Ravel^c, Melaine Le
6 Roy^c, Philip Deline^c, Vincent Favier^d, Jean-François Buoncristiani^e, ASTER Team^a

7

8 ^a Aix-Marseille Univ, CNRS, IRD, INRA, Coll France, CEREGE, Aix-en-Provence, 13545,
9 France

10 ^b Université Grenoble Alpes, Université Savoie Mont Blanc, CNRS, ISTerre, Chambéry,
11 73000, France

12 ^c Université Grenoble Alpes, Université Savoie Mont Blanc, CNRS, EDYTEM, Chambéry,
13 73000, France

14 ^d Université Grenoble Alpes, CNRS, IRD, Grenoble INP, IGE, Grenoble, France

15 ^e Biogéosciences, UMR 6282 CNRS, Université Bourgogne Franche-Comté, 6 Boulevard
16 Gabriel, Dijon, 21000, France

17

18 Consortium: ASTER Team (Georges Aumaître, Didier Bourlès, Karim Keddadouche)

19

20 Correspondence to: Marie Protin (protin@cerege.fr)

21

22 **Abstract**

23 Investigation of Holocene extents of mountain glaciers along with the related naturally-driven
24 climate conditions helps improve our understanding of glacier sensitivity to ongoing climate

25 change. Here, we present the first Holocene glacial chronology in the Mont-Blanc massif
26 (Argentière glacier) in the French Alps, based on 25 *in situ*-produced cosmogenic ¹⁰Be dates
27 of moraines and glacial bedrocks. The obtained ages from mapped sequences of moraines at
28 three locations reveal that the glacier was retreating from its Lateglacial extent and oscillating
29 several times between ~11.7 ka and ~10.4 ka, i.e. during the Younger Dryas/Early Holocene
30 (YD/EH) transition, before substantially retreating at ~10.4 ka. Climate conditions
31 corresponding to the past extents of Argentière glacier during the YD/EH transition (~ 11 ka)
32 and the Little Ice Age (LIA) were modelled with two different approaches: by determining
33 summer temperature differences from reconstructed ELA-rises and by using a Positive
34 Degree Day (PDD) mass-balance model coupled with a dynamic ice flow model. The ELA-
35 rise reconstructions yield a possible range of summer temperatures for the YD/EH transition
36 that were cooler by between 3.0 and 4.8°C compared to the year 2008, depending on the
37 choice of the ELA sensitivity to summer temperature. The results from the PDD model
38 indicate temperatures cooler by ~3.6 to 5.5°C during the YD/EH transition than during the
39 1979-2002 period. For the LIA, our findings highlight that the role of local precipitation
40 changes, superimposed on the dominant temperature signal, is important in the detailed
41 evolution of the glacier. Overall, this study highlights the challenge that remains in accurately
42 inferring paleoclimate conditions from past glacier extents.

43

44 **Keywords**

45 Holocene; Glaciation; Western Europe; Cosmogenic nuclides; Glacier fluctuations; French
46 Alps; Moraine dating; Paleoclimate reconstruction; PDD modeling

47

48 **1. Introduction**

49 Investigating natural climate changes during the Holocene is relevant for assessing the impact
50 of the current climate changes, because Holocene climate variations were similar in amplitude
51 to the ones that are historically observed and predicted for the next few decades (e.g. Marcott
52 et al., 2013). Mountain glaciers are known to be sensitive climate change indicators
53 (Oerlemans, 2005), as their dynamics in the mid-latitudes, e.g. in the European Alps, depend
54 both on summer temperature and winter precipitation variations. They thus represent a highly
55 useful proxy for Holocene climate reconstructions. The ongoing trend of global glacier
56 retreat, which started after the end of the Little Ice Age (LIA), in the middle of the 19th
57 century, is well recorded with instrumental measurements (Leclercq et al., 2014). Evidence of
58 pre-instrumental glacier fluctuations are recorded by glacial landforms, which provide the
59 opportunity to reconstruct past glacier chronologies and examine glacier-climate interactions
60 over a longer period. In particular, moraine deposits give valuable information about past
61 glacier extents and dating them using *in situ* cosmogenic nuclides allows us to put glacier
62 variations into a spatio-chronological framework. Over the past few years, a growing number
63 of studies in the Alps have reported advanced glacier positions during the Late Glacial and
64 Holocene relying on *in situ*-produced cosmogenic beryllium-10 (¹⁰Be) moraine dating (e.g.
65 Moran et al., 2016; Schimmelpfennig et al., 2014; Schindelwig et al., 2012). In several of
66 these studies, the corresponding equilibrium line altitudes (ELA) were estimated (e.g. Baroni
67 et al., 2017; Hofmann et al., 2019; Le Roy et al., 2017). As the ELA directly depends on the
68 climate, in particular on atmospheric temperature and precipitation, reconstruction of past
69 ELAs provides the opportunity to estimate paleoclimate conditions. Atmospheric temperature
70 variations can be inferred using the adiabatic lapse rate or an ELA sensibility to atmospheric
71 temperature, as has previously been done in the Alps by Hofmann et al. (2019), Le Roy et al.
72 (2017) and Moran et al. (2016). However, this approach assumes that the impact of
73 precipitation on the glacier behavior is negligible or that the precipitation amount did not

74 change through time, potentially leading to a bias in the deduced temperature variations. In
75 the Alps, only few studies have attempted so far to infer precipitation changes from past
76 glacier extents (e.g. Keeler, 2015; Kerschner and Ivy-Ochs, 2007), as disentangling the
77 detailed contributions of both precipitation and temperature changes to glacier fluctuations is
78 still difficult (Solomina et al., 2016).

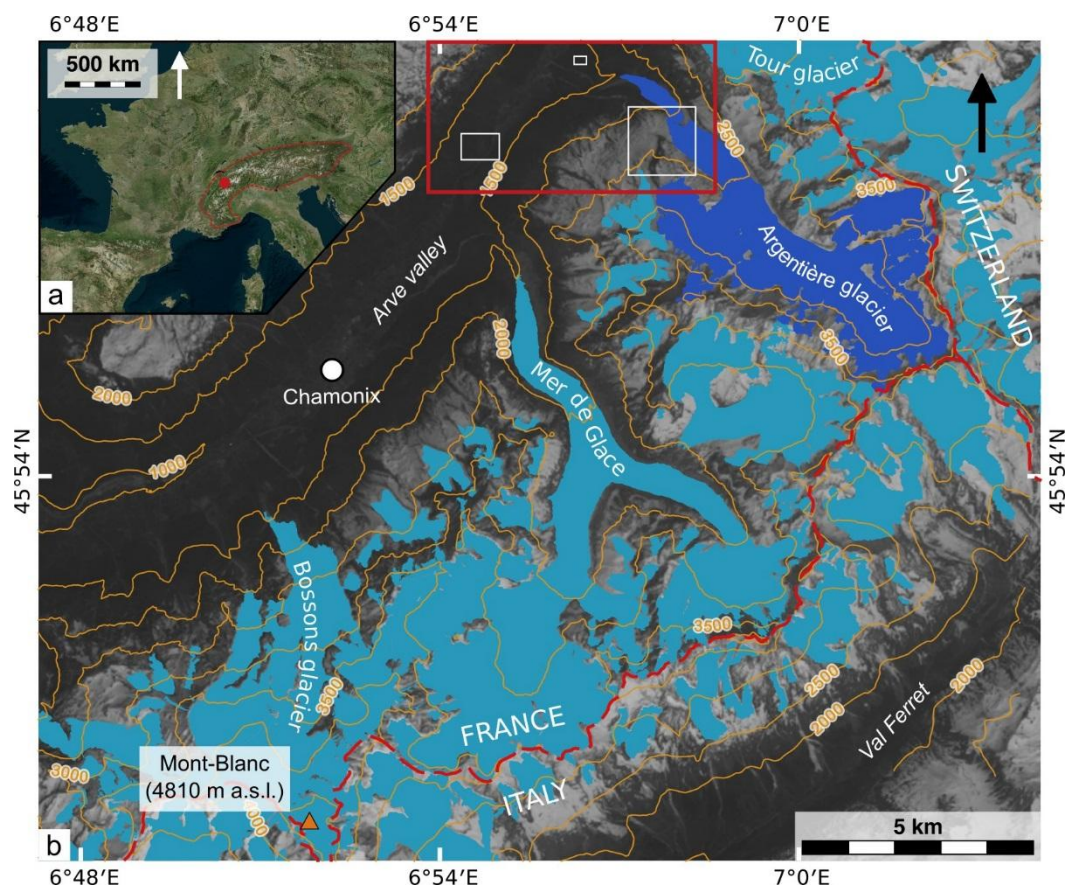
79 In this study, we explore the frontal and lateral moraines, as well as roches moutonnées
80 located beyond the limits of the LIA extent of Argentière glacier with the objective to present
81 the first alpine Holocene glacier chronology based on ^{10}Be dating in the Mont-Blanc massif.
82 Potential climatic conditions corresponding to past extents of Argentière glacier are
83 determined using two different approaches, including a PDD mass-balance model, which
84 allows considering both precipitation and temperature variations.

85

86 **2. Study site, geomorphologic setting and previous work on the past fluctuations of** 87 **Argentière glacier**

88 Argentière glacier (45°55'N, 6°57'E), located on the north-western side of the Mont Blanc
89 massif, is the second largest glacier in the French Alps (Figure 1). In 2008, it covered a
90 surface of $\sim 14 \text{ km}^2$ with a length of almost 10 km and an altitude range spanning 3530 m to
91 1550 m a.s.l. (Six and Vincent, 2014; Vincent et al., 2009). Since 2009, the tongue (7 % of the
92 glacier area) is disconnected from the main glacier body and remains fed by an icefall located
93 at ~ 2200 m a.s.l. This tongue is covered by debris since at least the middle of the 20th century
94 (aerial photography from IGN, <https://remonterletemps.ign.fr>), while it was uncovered in the
95 middle of the 19th century according to pictorial documents from the LIA (Fontaine, 2015).
96 The ELA has been measured at ~ 2890 m a.s.l. between 1995 and 2011 (Six and Vincent,
97 2014). The mean annual temperature and precipitation were 6.5°C and 1238 mm in Chamonix
98 - Le Bouchet, the nearest weather station located at 1042 m a.s.l. for the time period 1961-

99 1990 (Météo France) and are estimated at 1.8°C and 1783 mm at ~2000 m a.s.l. next to
 100 Argentière glacier for the time period 1979-2002 (Joly et al., 2018 and personal
 101 communication of D. Joly). Snow accumulation on the glacier at 3000 m a.s.l. is known to be
 102 3 times larger than valley precipitation due to the orographic effect on precipitation, impact of
 103 the wind and of avalanches, as the glacier is surrounded by steep slopes (Six and Vincent,
 104 2014). Climatic data began to be collected in the Alpine region in the year 1760 (temperature
 105 measurements) and in the year 1800 (precipitation) and are compiled in the HISTALP project
 106 (<http://www.zamg.ac.at/histalp/>; Auer et al., 2007).

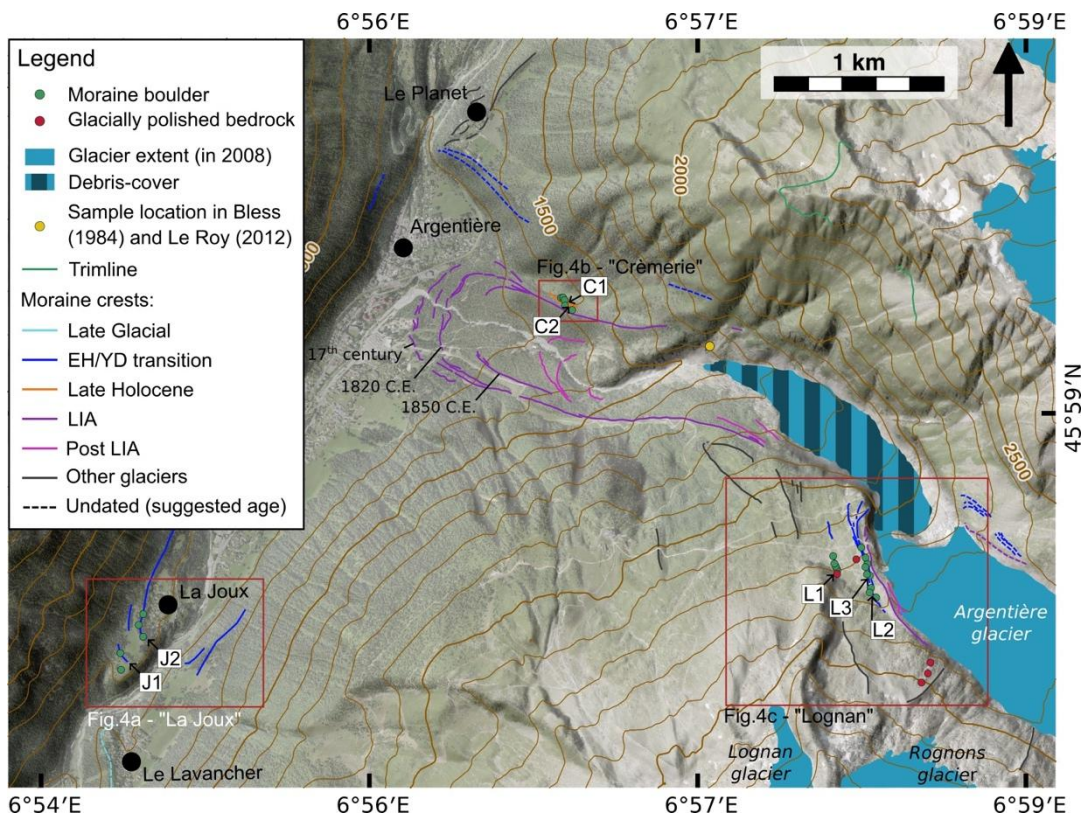


107
 108 *Figure 1 : General overview of the study area. (a) Location of the Mont Blanc massif (red*
 109 *dot) in the Alps (red dotted line). (b) Landsat 8 image of the Mont Blanc massif from April*
 110 *2005, with the 2008 extent of glaciers in blue. French glaciers: Gardent et al. (2014); Swiss*
 111 *glaciers: Fischer et al. (2014); Italian glaciers: Smiraglia et al. (2015). Argentière glacier is*
 112 *highlighted in dark blue. Red dotted lines represent countries borders. Red square represents*

113 *the location of Figure 2 and white squares represent the sampling locations, shown in Figure*
114 *7.*

115 The Argentière glacier catchment is mainly formed by granite from the late Hercynian along
116 with Variscan metamorphic rocks (Bussy et al., 2000). Numerous preserved moraine ridges
117 and moraine remnants are visible in the catchment, close to the glacier, and downstream in the
118 Arve valley providing evidence of the past fluctuations of Argentière glacier (Figure 2).
119 While it's behavior since the LIA is well-known (Bless, 1984; Payot, 1884; Vincent et al.,
120 2009), few chronological data constrain its Holocene fluctuations prior to the 17th century
121 (Bless, 1984; Le Roy, 2012). During the Last Glacial Maximum (LGM), the valleys around
122 the Mont Blanc massif were glacierized, and the glacier surface reached an altitude of 2400 m
123 a.s.l. at the location of Argentière glacier, as reconstructed from the trimline positions in the
124 region of the Mont Blanc massif (Figure 2, Coutterand and Buoncristiani, 2006). During the
125 Late-Glacial, glaciers located on the western flank of the Mont-Blanc massif were still
126 connected as one glacier named Arve glacier, extending in the Arve valley over a distance of
127 30 km, where numerous and mostly lateral moraine relicts attest to multiple glacier
128 fluctuations during that period (Coutterand and Nicoud, 2005). At one point during the retreat
129 from the large Late-Glacial glacier extents, Argentière glacier disconnected from its neighbors
130 Mer de Glace and Tour Glacier, which is revealed by two latero-frontal moraines sets near *La*
131 *Joux* et near *Le Planet* in the Arve valley (Figure 2). Due to the lack of direct dating methods,
132 20th century studies on past glacier fluctuations were often based on the comparison of ELA
133 depressions, geomorphic moraine characteristics, pollen analyses or limiting radiocarbon
134 dates to correlate moraines within regionally defined relative glacier chronologies like the
135 “stadials” of the classical Swiss alpine terminology (e.g. Maisch, 1981). Such relative dating
136 was applied to the extent of Le Tour and Argentière glaciers and several interpretations
137 suggest that these moraines were deposited during the Late-Glacial or Early Holocene (Jaillet

138 and Ballandras, 1999; Lucéna and Ballandras, 1999; Bless, 1984), although there is no
 139 indication for an univocal correlation to the classical Swiss alpine nomenclature. Further
 140 evidence of Argentière glacier variations during the Holocene are provided by Bless (1984)
 141 and Le Roy (2012). Radiocarbon dating of subfossil organic material found in stratigraphic
 142 position in the right-lateral composite moraine (yellow dot on Figure 2) gave evidence of five
 143 glacier advances between ~4 ka and 1.2 ka, *i.e.* during the so-called Neoglacial, a period when
 144 the climatic conditions became more suitable for glacial advances (Bless, 1984). In the same
 145 moraine profile, dating of detrital wood embedded-in-till 30 years later, indicates an advance
 146 during the 9th century, similar in elevation to the LIA maxima (Le Roy, 2012). Finally,
 147 Argentière glacier reached its LIA frontal maximum extent during the 17th century, according
 148 to several written reports about the destruction or menace of villages by the advancing glacier
 149 (Bless, 1984).



150
 151 *Figure 2 : Geomorphic map of the study area with individual sample locations on the 5 m*
 152 *IGN DEM RGE ALTI. The 2008 extent of Argentière and nearby glaciers are represented in*

153 *blue (Gardent et al., 2014). Geomorphologic features were mapped based on Bless (1984)*
154 *and Le Roy (2012), DEM interpretation and field observations. Dashed lines represent*
155 *undated moraines, their ages are presumed from their position relative to moraines of known*
156 *ages; grey lines are moraines attributed to nearby glaciers.*

157

158 **3. Methodology**

159 **3.1. Moraine mapping**

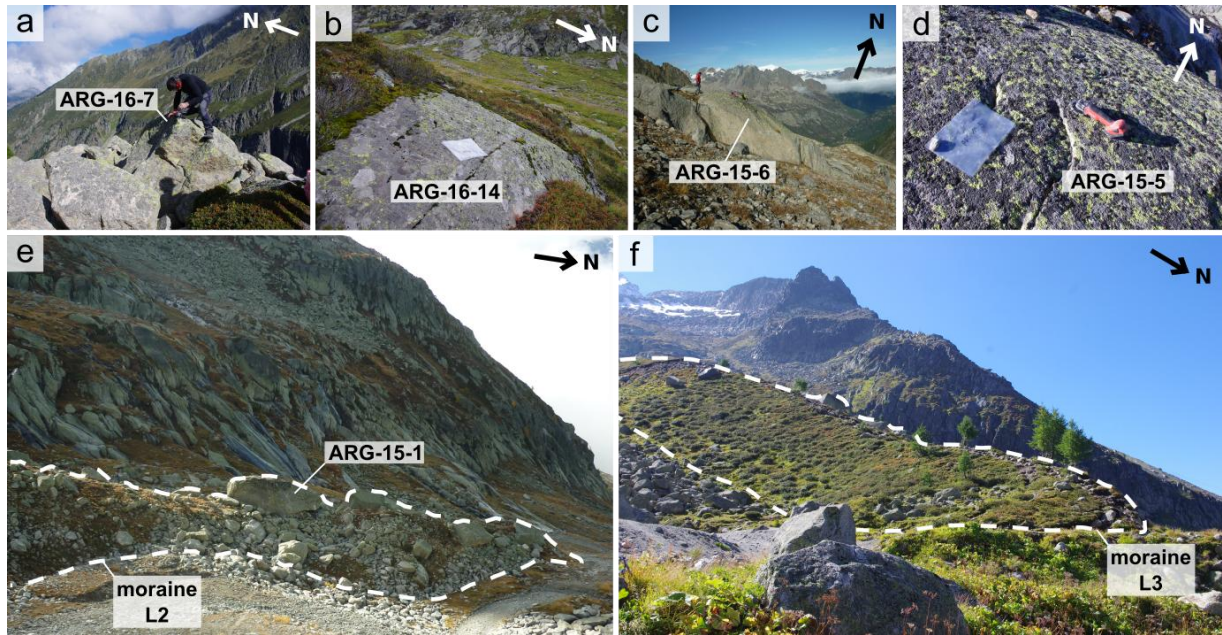
160 The geomorphologic map presented in Figure 2 was produced using Geographic Information
161 System (GIS). It is based on field observations along with interpretation of recent aerial
162 images (from the IGN, 50 cm resolution) and LIDAR digital elevation models (DEM), with
163 resolution of 1 m (Arve valley) and 2 m (Argentière catchment). The map in Figure 2 also
164 includes moraines that were mapped in earlier studies (Le Roy, 2012; Bless, 1984).

165 **3.2. Sampling and cosmogenic ^{10}Be ages**

166 All samples were obtained using a cordless angle grinder, chisel and hammer (Figure 3).
167 Boulder samples were collected from the top of boulders embedded in the crests or on the
168 slopes of selected moraines and bedrock samples were preferentially taken from sloping
169 surfaces to minimize the risk of cover by vegetation, sediment or snow (Figure 3). We only
170 sampled surfaces with minimal signs of erosion, exhibiting glacial striation when possible,
171 and moraine boulders that were big enough (>1 m) to avoid the risk of exhumation. In total,
172 20 moraine boulders and 5 bedrock samples were collected. Topographic shielding was
173 determined in the field using a clinometer.

174 The chemical procedure for ^{10}Be extraction from the rock was conducted at CEREGE (Aix-
175 en-Provence, France). Samples were crushed and sieved to the 250-500 μm fraction. Quartz
176 was isolated from other grains first by magnetic separation, then either by repeated leaching

177 in a $\text{H}_2\text{SiF}_6/\text{HCl}$ mixture or by froth flotation, and finally by at least three sequential leaching
178 steps in concentrated HF to remove remaining feldspar grains and atmospheric ^{10}Be . About
179 0.1 g of a 3025 ± 9 ppm in-house ^9Be carrier solution (Merchel et al., 2008) was added to the
180 purified quartz before its complete dissolution in concentrated HF. Beryllium was extracted
181 and purified by separation on anion and cation columns and by successive alkaline
182 precipitations of $\text{Be}(\text{OH})_2$, and the samples were then oxidized for one hour at 700°C . The
183 final BeO oxides were mixed with Nb powder and loaded into nickel cathodes for AMS
184 measurements. The $^{10}\text{Be}/^9\text{Be}$ ratios of all samples were measured at the French national AMS
185 facility ASTER (Arnold et al., 2010) and calibrated against in-house standard STD-11 with an
186 assigned $^{10}\text{Be}/^9\text{Be}$ ratio of $(1.191 \pm 0.013) \times 10^{-11}$ (Braucher et al., 2015) using the ^{10}Be half-
187 life of $(1.387 \pm 0.0012) \times 10^6$ years (Chmeleff et al., 2010; Korschinek et al., 2010).
188 Analytical uncertainties due to AMS measurement include ASTER counting statistics and
189 stability (~ 0.5 %; Arnold et al. (2010)) and blank correction. Correction for the chemical
190 blanks, whose $^{10}\text{Be}/^9\text{Be}$ ratios range between $(3.21 \pm 0.50) \times 10^{-15}$ and $(4.87 \pm 0.63) \times 10^{-15}$,
191 were performed by subtracting their numbers of atoms ^{10}Be from those of the samples
192 calculated from the $^{10}\text{Be}/^9\text{Be}$ ratios (Table 1).



193

194 *Figure 3 : Photographs of sample sites at Argentière glacier. Example of (a) moraine boulder*
 195 *(ARG-16-7), (b) inter-morainic bedrock surface and (c) roche moutonnée (ARG-15-6) along*
 196 *with (d) roche moutonnée surface (ARG-15-5) sample from Lognan area. View of dated*
 197 *moraines (e) L2 and (f) L3 (framed by the dashed line) located in the left-lateral Lognan area.*

198 Surface exposure ages were calculated with the CREp online calculator (Martin et al., 2017)
 199 applying the Lal-Stone time corrected scaling scheme, the ERA40 Atmosphere model and the
 200 Atmospheric ^{10}Be -based VDM for geomagnetic database (see Martin et al. (2017) and
 201 references therein). The “Alpine” ^{10}Be production rate of 4.11 ± 0.10 atoms $^{10}\text{Be}/\text{g}$
 202 established by Claude et al. (2014) was retained here as it is the only available regional
 203 production rate. In addition, it yields results very similar to the NENA production rate (Balco
 204 et al., 2009), which has often been used in previous studies in the Alps and has a value of 4.10
 205 ± 0.17 atoms $^{10}\text{Be}/\text{g}$ when recalculated in CREp with the above parameters. We note that the
 206 “Arctic” production rate (Young et al., 2013; 4.12 ± 0.25 atoms $^{10}\text{Be}/\text{g}$ according to CREp),
 207 also used for several alpine studies, would lead to ages younger by ~ 0.25 %. Calculated
 208 exposure ages are presented in Table 1. We did not correct the ages for snow cover effects or
 209 surface erosion, as these effects were minimized by sampling boulders least likely to have

210 been snow covered and with minimal signs of erosion. Applying a high snow cover correction
211 corresponding to 50 cm of snow for 6 months, as used in Chenet et al. (2016), would lead to
212 ages older by $\leq 8\%$ and assuming an erosion rate of 1 mm.kyr^{-1} (André, 2002) would lead to
213 ages older by only 1%. Nonetheless, the presented ages should be considered minimum
214 exposure ages.

215 **3.3. Glacier reconstruction and paleoclimatic modelling**

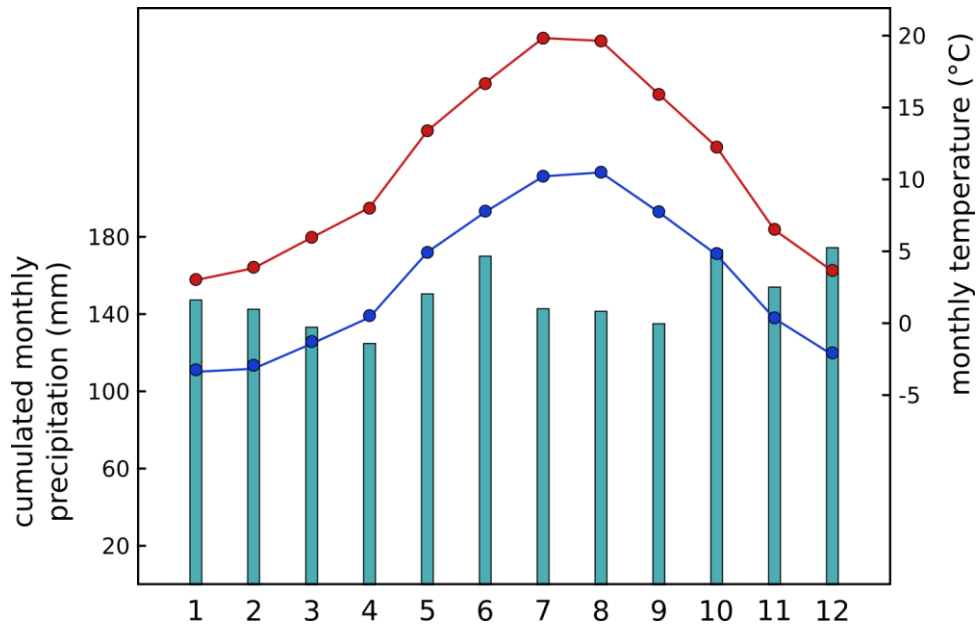
216 Two approaches were used to infer paleoclimatic conditions from the extents of Argentière
217 glacier. Both approaches are based on the simplified assumption that the glacier is in
218 equilibrium with the climate conditions during the respective present-day reference periods
219 detailed below.

220 *3.3.1. GIS-based ELA reconstruction and paleo-temperature determination*

221 In the first approach, 3D glacier surface reconstructions were generated for different glacier
222 extents in the past using the ArcGIS toolbox GlaRe (Pellitero et al., 2016) based on the
223 mapping of the moraines presented in Figure 2. The topography of the bedrock beneath of
224 Argentière glacier used for the reconstruction was determined by subtracting the ice thickness
225 (Rabatel et al., 2018) from the 25 m IGN DEM BD Alti. ELA calculations were then done
226 using the ArcGIS toolbox developed by Pellitero et al. (2015) according to the Area-Altitude
227 Balance Ratio (AABR) with a balance ratio of 1.59 and the Accumulation Area Ratio (AAR)
228 method with a ratio of 0.67, both values representative for the Alps (Pellitero et al., 2015;
229 Rea, 2009). While the AAR method is simply based on the ratio between the surface of the
230 accumulation area and the surface of the entire glacier, the AABR method take into account
231 the hypsometry of the glacier (Osmaston, 2005) and the mass balance gradient (Benn and
232 Lehmkuhl, 2000) and is therefore considered more reliable to approximate ELAs (Lukas,
233 2007; Pellitero et al., 2015). However, the AAR method has most often been used in the Alps
234 (e.g. Hofmann et al., 2019; Le Roy et al., 2017; Moran et al., 2016). Thus, for the

235 paleoclimatic discussion we prefer the results inferred from the ELAs calculated with the
236 AABR method and the results from the AAR method are only used for the sake of
237 comparison with other Alpine sites. We adjusted the shear stress value along the flowlines in
238 the ArcGIS toolbox GlaRe (Pellitero et al., 2016) by comparing the ELA calculated for the
239 2008 extent of Argentière glacier to the mean ELA measured in the field between 1995 and
240 2011 (~2890 m, Six and Vincent, 2014). The best estimate are found for a shear stress value
241 of 150 kPa and an automatic shape factor. The calculated ELAs for the 2008 extent are 2866
242 m using the AABR method and 2801 m using the AAR method. These two values are close,
243 yet inferior, to the measured ELA. It has to be noted that in 2008 the glacier was not in
244 steady-state, therefore the measured ELA does not reflect an equilibrium position unlike the
245 calculated values, which hinders us from accurately fitting both and might explain the
246 difference between them.

247 The difference of the resulting paleo-ELAs between two periods allows for determination of
248 the associated variation in atmospheric temperature (T) by using a constant ELA sensitivity to
249 atmospheric temperature (S) and assuming the same precipitation as today, following the
250 equation $\Delta T = \Delta ELA/S$. The ELA sensitivity to summer temperature is nonetheless difficult
251 to estimate and two values are used in this paper: $115 \text{ m}^\circ\text{C}^{-1}$, which is relevant for French
252 Alpine glaciers (Rabatel et al., 2013); and $72 \text{ m}^\circ\text{C}^{-1}$, which was empirically quantified for
253 Argentière glacier by Six and Vincent (2014) and takes into account the local effects of
254 temperature and all meteorological parameters that influenced the snow and ice ablation.



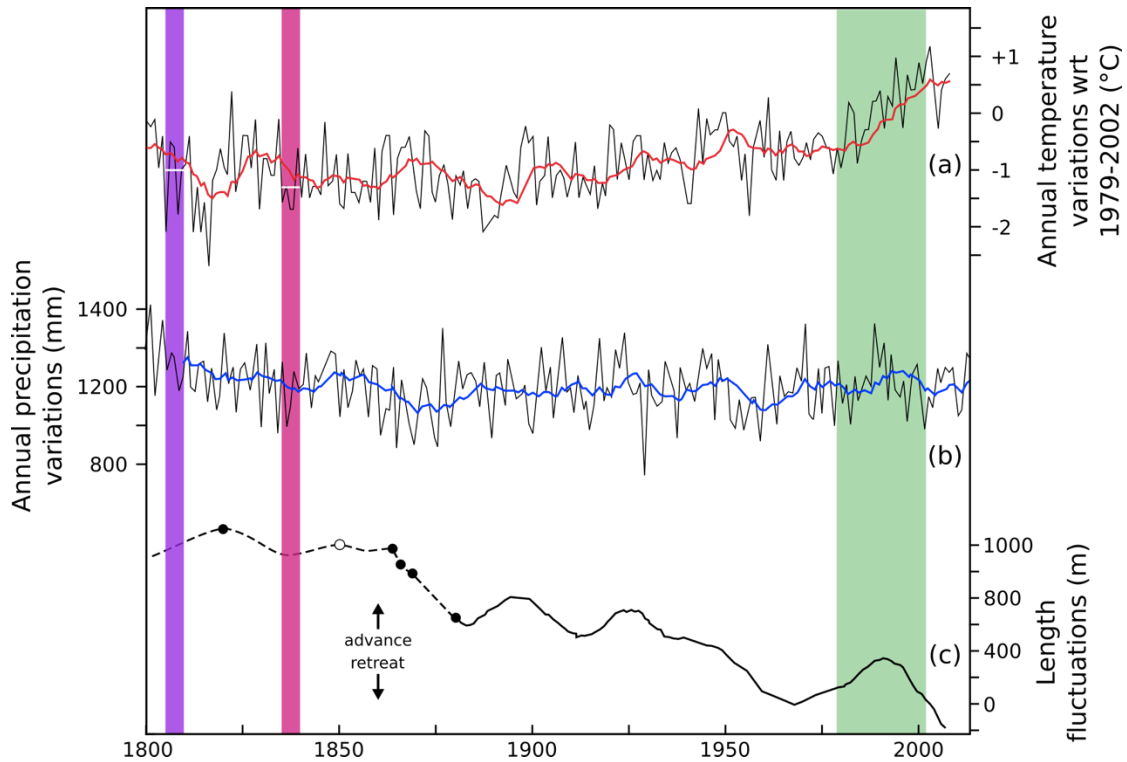
255

256 *Figure 4 : Climatic data of Argentière glacier between 1979 and 2002 at ~2000 m a.s.l.. Blue*
 257 *bars represent the cumulated monthly precipitation, the blue and red curves represent*
 258 *respectively the minimum and maximum monthly temperatures. 1 to 12 represents the months*
 259 *January to December.*

260 3.3.2 PDD modelling

261 In the second approach, combinations of precipitation and temperature variations and ELAs
 262 for different glacier extents were determined by using a PDD mass-balance model coupled
 263 with a dynamic ice flow model, described in Blard et al. (2007). This model has previously
 264 been used for glaciers in the central pacific by Blard et al. (2007), in the Andes by Jomelli et
 265 al. (2011) and in Greenland by Biette et al. (2018). The topography of the watershed of
 266 Argentière glacier used for the modeling is the same used for the GIS-based reconstructions
 267 (see section 3.3.1.). The model was calibrated using the mass-balance data from 1979 to 2002
 268 (considered here as the present-day reference period) collected at Argentière glacier by the
 269 GlacioClim Network (<https://glacioclim.osug.fr>) from extensive field measurements on 10
 270 markers distributed along the glacier (5 in the ablation area and 5 in the accumulation area)
 271 and local monthly values of temperature and precipitation for the same period (personal

272 communication of D. Joly), inferred at 2000 m a.s.l. in the Argentière catchment from a
273 downscaling method based on a geomatic spatial model (Joly et al., 2018). Figure 4 depicts
274 the monthly values of temperature and precipitation of Argentière glacier averaged from 1979
275 to 2002 as used in the model. This interval is nearly twice as long as the 10-14 years response
276 time of the glacier front position to a mass balance change (Vincent et al., 2009) and is long
277 enough to fade out the inter-annual variability. In addition, the glacier length at the beginning
278 of this period is very similar to that at the end, as it includes an advance of the glacier
279 followed by an equal retreat (Figure 5). This consolidates the assumption that the glacier was
280 roughly in equilibrium with the mean climatic condition during this period. This period is put
281 into a broader context and compared to the variations of Argentière glacier since 1800 in
282 Figure 5. The atmospheric lapse rate of temperature and precipitation are fixed at $0.65^{\circ}\text{C}/\text{m}$
283 and $80\text{mm}/100\text{m}/\text{year}$, respectively. This precipitation lapse rate matches best the field data
284 taking into the range of the precipitation lapse rate between precipitation in the valley and at
285 high altitude in the MMB of $52\text{mm}/100\text{m}/\text{years}$ (Corbel, 1963) as well as the variable ratio
286 between valley precipitation and winter accumulation on Argentière glacier (Six and Vincent,
287 2014) equivalent to a lapse rate of $\sim 95\text{mm}/100\text{m}/\text{years}$.

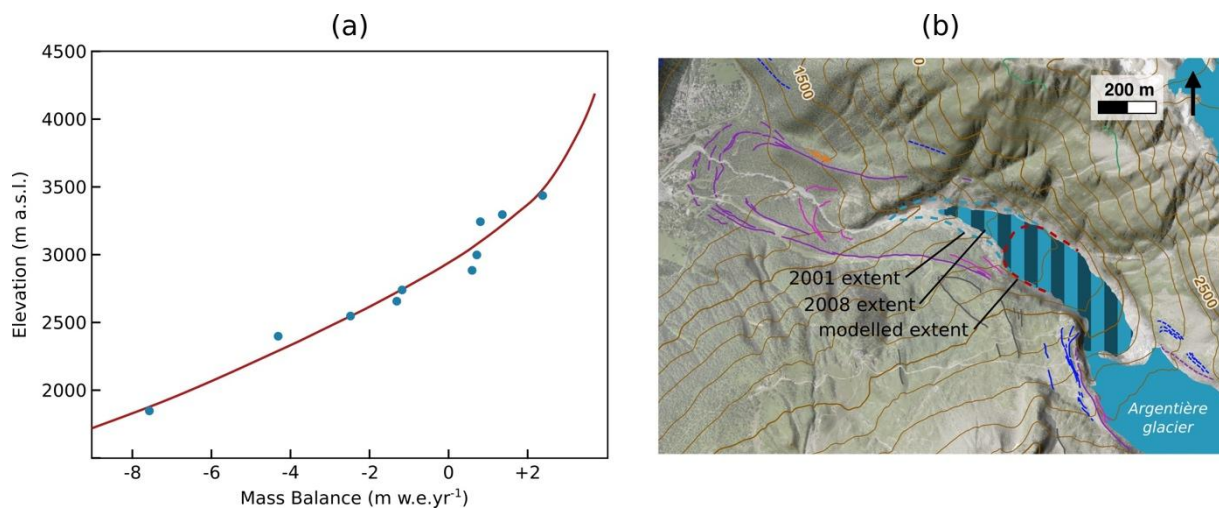


288

289 *Figure 5 : (a) Annual temperature anomalies (reference period 1979-2002); (b) annual*
 290 *precipitation in the west part of the Alps from the HISTALP time series (Auer et al., 2007)*
 291 *and (c) front variation of the Argentière glacier - the origin of the axis is arbitrary (1818-*
 292 *1880: Payot, 1884 in Fontaine, 2015; 1850: Bless (1984); 1880-2000: Francou and Vincent,*
 293 *2007; > 2000: Vincent et al., 2009. Red and blue curves represent 10-years running means.*
 294 *Period of reference of the climatic data of Argentière glacier (1979-2002) used as input in the*
 295 *PDD model is highlighted in green. Periods considered for extracting the temperature values*
 296 *for the 1820 and 1850 glacier extents, accounting for the glacier's response time, are*
 297 *highlighted in purple and pink, respectively. The extracted mean temperatures are depicted by*
 298 *white horizontal lines.*

299 Figure 6 shows the correlation between observed and calculated mass balance of Argentière
 300 glacier. This best fit ($R^2 = 0.97$) was obtained using the least mean square optimization on the
 301 determination of the melting factor (MF) used in the PDD model, whose values are $MF_{\text{snow}} =$
 302 $2.3 \text{ mm w.e. } ^\circ\text{C}^{-1} \text{ d}^{-1}$ and $MF_{\text{ice}} = 5.1 \text{ mm w.e. } ^\circ\text{C}^{-1} \text{ d}^{-1}$. These values are close to the ones

303 defined in Réveillet et al. (2017) for Argentière glacier: $MF_{\text{snow}} = 3.5 \text{ mm w.e. } ^\circ\text{C}^{-1} \text{ d}^{-1}$ and
304 $MF_{\text{ice}} = 5.5 \text{ mm w.e. } ^\circ\text{C}^{-1} \text{ d}^{-1}$. Using these parameters and the climatic inputs presented in
305 Figure 4, the calculated ELA is 2940 m a.s.l., whereas Argentière glacier ELA measurements
306 using satellite images during the years 1984 to 2002 ranged between 2623 and 2861 m a.s.l.
307 (Rabatel et al., 2013). Furthermore, the length of the modeled glacier is between 600 and 300
308 m shorter than that of Argentière glacier between 1990 and 2001. As the lower part of the
309 Argentière glacier is covered by debris from before the middle of the 20th century, and termini
310 of debris-covered glaciers, like the Miage glacier in the Mont Blanc massif (Smiraglia et al.,
311 2010), are often less responsive to climatic variability than non-covered glaciers (Scherler et
312 al., 2011), this might be the reason why the model predicts a shorter length. Nonetheless, due
313 to the excellent agreement between calculated and measured mass balance (Figure 6), we
314 consider that the above calibration of the model is suited for modeling the past extents of the
315 glacier. For each investigated extent, the model considers all potential combinations of
316 precipitation and temperature conditions that lead to a match of the front of the modeled
317 paleo-glacier with the position of the corresponding frontal moraine mapped in the field.
318 ELAs correspond to the altitudes where the glacier mass balance is zero. For each glacier
319 extent, ELAs vary over a range of more than 100 m, due to the large range of assumed
320 precipitation conditions (between 0 and 2 times that of the reference period).



321
 322 *Figure 6: (a) Comparison between observed mass balance (1979-2002; Glacioclim Network)*
 323 *on the Argentière glacier (blue dots) and mass balance calculated by the PDD model (red*
 324 *curve). (b) Comparison between the modelled glacier extent for the reference period of 1979-*
 325 *2002 (red dotted line), the 2001 extent (blue dotted line; Le Roy, 2012) and the 2008 extent*
 326 *(blue area; Gardent et al., 2014).*

327
 328 **4. Results**

329 **4.1. Description of the geomorphological evidence**

330 Figure 2 presents a moraine map of the Argentière catchment. The frontal moraines located
 331 around 1.5-2 km downstream of the present glacier front (purple moraines in Figure 2) have
 332 been assigned by Bless (1984) to four LIA advances between the 17th century and 1850 based
 333 on analysis of historical written documents and paintings combined with lichenometry dating.
 334 On both lateral sides, the LIA advances are represented by massive composite moraines of up
 335 to 80 m height and ≥ 1 km length. Multiple ridges are visible between the ~1850 frontal
 336 moraine and the current front, representing the generally gradual retreat of the glacier since
 337 the end of the LIA (pink moraines in Figure 2). Immediately to the north, slightly outboard of
 338 the right-lateral LIA composite moraine, four short ridges of so far unknown age are
 339 preserved (orange moraines in Figure 2). This area, hereafter called “Crèmerie”, is covered by

340 a dense conifer forest, but the morphology of the ridges is noticeable on the DEM and attested
341 by a few disseminated moraine boulders.

342 Further upstream near the present-day Argentière glacier icefall, multiple ridges of lateral
343 moraines are preserved. On the left-lateral side, in the area called “*Lognan*”, the most
344 prominent moraine, ~15 m-high and 700 m-long is attributed to the LIA (Figure 2). Only a
345 few tens of meters outboard, two dissected main ridges and several subridges lie tight together
346 (among them L2 and L3 in Figure 2), and another dissected ridge is preserved about 150-200
347 m further outboard (L1 in Figure 2). According to their positions, these ridges are pre-LIA
348 moraine relicts but were undated until now. They display a smoother morphology than the
349 massive LIA moraine, but are located around the same altitude, and exhibit several boulders
350 suitable for sampling. At their upstream (southern) ends, these moraines abut against a steep
351 and up to a 150 m-high bedrock outcrop, which testifies to past glacial cover owing to
352 numerous roches moutonnées (Figure 3). This roche moutonnée area lies between the current
353 terminus of Rognons glacier and the left-lateral bank of Argentière glacier and is framed by
354 two moraines deposited by Rognons glacier during its retreat. A similar moraine sequence
355 pattern is observed on the north-eastern bank of the glacier. Moraines located further to the
356 west of the pre-LIA deposits in the Lognan area (grey moraines on Figure 2) are not
357 considered as moraines built by Argentière glacier. They were most likely deposited by the
358 Lognan glacier, a smaller nearby glacier. This is suggested by their composition of gneiss
359 boulders, transported from the Lognan glacier catchment, whereas the boulders embedded in
360 the sampled moraines are granitic according to the main lithology of the Argentière glacier
361 catchment.

362 Downstream in the Arve valley near *La Joux*, relicts of a latero-frontal moraine set are
363 preserved (dark blue moraines in Figure 2). These moraines, smooth and covered by conifer
364 trees, were studied and mapped in detail by Bless (1984) and Lucéna and Ballandras (1999)

365 and named “La Chauffria II” and “La Joux” (Lucéna and Ballandras, 1999), corresponding to
366 J1 and J2 moraines respectively in Figure 2. Furthermore, remnant of at least one other
367 moraine is located between J1 and J2. Some boulders are embedded in these moraines. A set
368 of lateral ridges are observed along the right-lateral valley flanks on the NW side of the
369 Argentière glacier catchment, especially south of *Le Planet*. North of these moraines, another
370 set of latero-frontal moraine relicts deposited by the neighbor Tour Glacier are visible near *Le*
371 *Planet* (Figure 2).

372 **4.2. Moraine and bedrock exposure ages**

373 All ^{10}Be exposure ages are listed in Table 1 and depicted in Figure 7. In the text, individual
374 exposure ages are presented with their 1σ analytical errors; in addition, Table 1 shows the 1σ
375 external errors, including the ^{10}Be production rate error. Before calculating the mean ages of
376 the glacial landforms, each age population was subject to a χ^2 test (2σ) to identify any
377 potential outliers. The landform ages correspond to the arithmetic means of the sample ages
378 and the uncertainties to their standard deviations (in the text and figures for internal
379 comparison); Table 1 also shows the errors that include the ^{10}Be production rate errors.
380 Probability plots of all boulder and moraine mean ages are illustrated in Figure 8.

381 Five samples from *La Joux* area yield ages between 13.2 ± 0.4 ka (LJX-17-5), corresponding
382 to an isolated boulder in front of the outmost moraine (J1), and 9.7 ± 0.3 ka (LJX-17-4),
383 which is the only age from J1 moraine. The mean age for the J2 moraine is 10.9 ± 0.9 ka ($n =$
384 2), after discarding sample LJX-17-1 (51.9 ± 2.7 ka) as an outlier. This latter boulder surface
385 was most likely affected by isotope inheritance from earlier periods of exposure to cosmic
386 radiation. Ages for the J1 and J2 frontal moraines are not in stratigraphic order, but the J1 age
387 relies upon only one sample, which might have been underestimated due to surface cover by
388 vegetation, erosion or anthropogenic impact, as the *La Joux* area is located in an area covered
389 by forest, close to a village.

Sample name	Latitude (dd)	Longitude (dd)	Altitude (masl)	Thickness (mm)	Shielding factor	Quartz weight (g)	Carrier (mg ⁹ Be)	Associated blank	¹⁰ Be/ ⁹ Be x10 ⁻¹⁴	[¹⁰ Be] (x 10 ⁴ at.g ⁻¹)	¹⁰ Be age (ka)	1σ analytical error (ka)	1σ external error (ka)
LOGNAN AREA													
MORAINES SAMPLE													
L1												11.66 ± 0.70 (0.76)	
ARG-16-9	45.96670	6.96065	2252	26	0.939	26.18	0.2979	30Jan17	35.8 ± 1.7	26.8 ± 1.3	12.21	0.58	0.64
ARG-16-10 (O)	45.96680	6.96056	2246	32	0.939	27.08	0.2996	30Jan17	29.9 ± 2.0	21.8 ± 1.5	10.10	0.64	0.68
ARG-16-11	45.96691	6.96050	2239	25	0.950	28.16	0.3008	30Jan17	33.0 ± 1.4	23.3 ± 1.0	10.63	0.42	0.48
ARG-16-12	45.96704	6.96041	2235	40	0.949	28.08	0.3062	30Jan17	35.8 ± 2.1	25.8 ± 1.5	11.88	0.68	0.73
ARG-16-13	45.96744	6.96031	2216	38	0.959	27.79	0.3012	30Jan17	36.1 ± 1.7	25.8 ± 1.2	11.93	0.55	0.61
L2												10.44 ± 0.19 (0.32)	
ARG-16-1	45.96575	6.96317	2287	20	0.970	27.84	0.2996	30Jan17	33.6 ± 2.2	23.8 ± 1.6	10.28	0.66	0.70
ARG-16-2	45.96575	6.96320	2274	50	0.970	27.55	0.2995	30Jan17	32.5 ± 2.1	23.3 ± 1.5	10.39	0.65	0.69
ARG-15-11	45.96551	6.96333	2265	45	0.969	12.75	0.3063	9Mai16	15.27 ± 0.47	23.87 ± 0.77	10.65	0.32	0.40
L3												10.41 ± 0.37 (0.45)	
ARG-16-3	45.96641	6.96312	2255	27	0.973	26.99	0.2993	30Jan17	32.9 ± 1.1	24.03 ± 0.79	10.61	0.33	0.41
ARG-16-4	45.96648	6.96289	2247	35	0.98	26.44	0.2993	30Jan17	31.7 ± 1.0	23.66 ± 0.77	10.52	0.32	0.40
ARG-15-12	45.96686	6.963	2235	22	0.974	18.27	0.3058	9Mai16	22.3 ± 0.7	24.41 ± 0.77	10.87	0.33	0.40

ARG-16-5 (O)	45.96703	6.96292	2234	20	0.971	27.98	0.3019	30Jan17	55.8 ± 5.0	39.9 ± 3.6	17.42	1.49	1.55
ARG-16-6	45.96736	6.96278	2216	50	0.971	28.00	0.3001	30Jan17	30.60 ± 0.95	21.60 ± 0.68	10.04	0.30	0.38
ARG-16-7	45.9679	6.96246	2189	30	0.971	28.63	0.3005	30Jan17	31.1 ± 1.1	21.50 ± 0.77	10.01	0.34	0.41

BEDROCK SAMPLE

ARG-15-5	45.96075	6.96705	2502	30	0.978	18.49	0.312	9Mai16	26.56 ± 0.96	29.6 ± 1.1	11.02	0.37	0.45
ARG-15-6	45.96123	6.96753	2465	20	0.977	9.37	0.3083	9Mai16	15.41 ± 0.57	33.2 ± 1.2	12.50	0.45	0.54
ARG-15-7	45.96181	6.96773	2427	35	0.974	8.09	0.3047	9Mai16	11.42 ± 0.41	27.9 ± 1.0	11.02	0.38	0.46
ARG-16-8	45.96650	6.96061	2384	25	0.485	13.25	0.2965	3Avril17	8.93 ± 0.46	12.86 ± 0.70	10.44	0.53	0.58
ARG-16-14	45.96727	6.96208	2252	28	0.969	20.20	0.2985	3Avril17	22.94 ± 0.96	22.3 ± 1.0	9.97	0.40	0.46

CREMERIE AREA

C1

ARG-17-1 (D)	45.98111	6.93959	1396	22	0.954	19.71	0.3009	3Avril17	1.79 ± 0.21	1.36 ± 0.22	1.16	0.19	0.21
ARG-17-2	45.98112	6.93975	1399	28	0.952	19.76	0.2903	3Avril17	1.55 ± 0.15	1.07 ± 0.16	0.90	0.14	0.14
ARG-17-3 (D)	45.98099	6.93985	1403	22	0.954	20.54	0.2817	3Avril17	1.65 ± 0.28	1.07 ± 0.26	0.89	0.23	0.23

C2

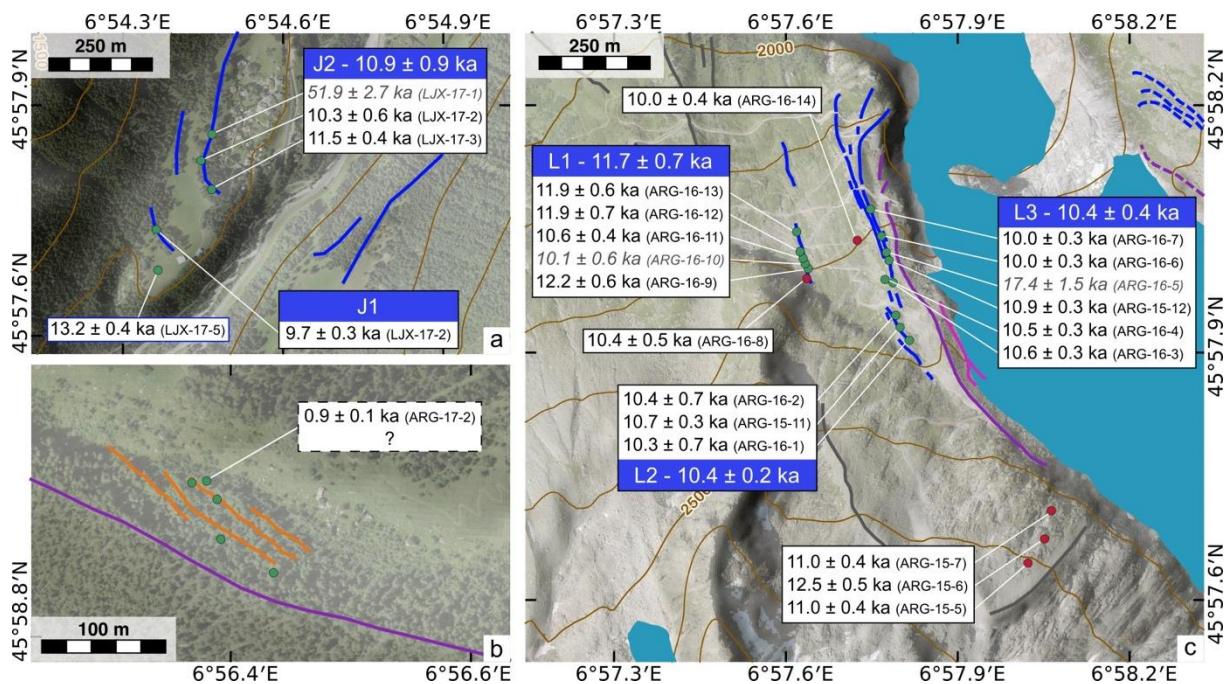
ARG-17-4 (D)	45.98070	6.93989	1407	36	0.960	20.16	0.2983	3Avril17	2.8 ± 3.3	2.32 ± 0.33	2.04	0.31	0.31
ARG-17-5 (D)	45.98046	6.94044	1408	28	0.956	20.47	0.2515	3Avril17	4.98 ± 0.47	3.64 ± 0.39	3.24	0.34	0.35

LA JOUX AREA

J2														10.93 ± 0.86 (0.90)
LJX-17-1 (O)	45.96437	6.90778	1214	24	0.955	12.01	0.2993	15Jan18	33.2 ± 1.6	54.7 ± 2.6	51.93	2.67	2.98	
LJX-17-2	45.96380	6.90743	1216	32	0.955	15.45	0.3091	15Jan18	8.28 ± 0.52	10.61 ± 0.69	10.32	0.64	0.68	
LJX-17-3	45.96318	6.90777	1213	41	0.955	23.66	0.3067	15Jan18	13.99 ± 0.53	11.82 ± 0.46	11.53	0.43	0.51	
J1														
LJX-17-4	45.96231	6.90604	1215	28	0.955	20.23	0.3007	15Jan18	10.41 ± 0.32	9.99 ± 0.32	9.70	0.30	0.38	
LJX-17-5	45.96139	6.90607	1209	48	0.955	21.63	0.3083	15Jan18	14.41 ± 0.45	13.4 ± 4.3	13.17	0.41	0.52	

BLANKS	Carrier (mg ⁹ Be)	¹⁰ Be/ ⁹ Be x10 ⁻¹⁴	¹⁰ Be (x 10 ⁴ at)
9Mai16	0.3068	0.321 ± 0.046	6.6 ± 1.0
30Jan17	0.3002	0.452 ± 0.057	9.1 ± 1.2
3Avril17	0.2788	0.487 ± 0.073	9.1 ± 1.4
15Jan18	0.3075	0.348 ± 0.050	7.2 ± 1.0

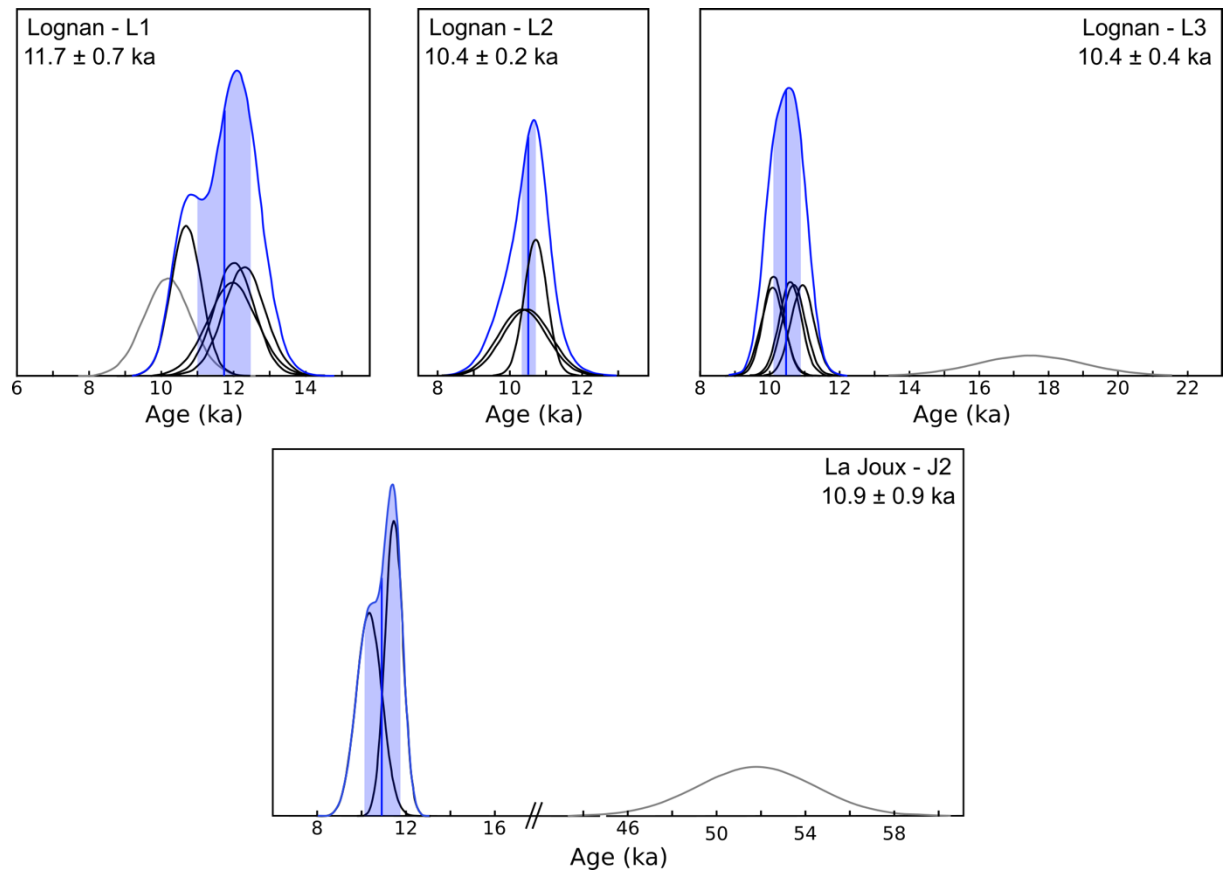
Table 1: Sample [A] and blanks [B] details, analytical data related to ¹⁰Be measurements and surface exposure ages. Outliers (O) were determined based on χ^2 test (2σ). Mean landform ages are also indicated with standard deviations and total uncertainties in parentheses. Samples from the Crèmerie area have been discarded (D) as the current were $<1\mu\text{A}$ and blank corrections $>50\%$.



391
 392 *Figure 7: Individual ^{10}Be exposure ages (white boxes) and mean ^{10}Be ages (colored boxes) of*
 393 *glacial landforms (moraines and glacially polished bedrock) in the study areas of the*
 394 *Argentière glacier (a) La Joux, (b) Crèmerie, and (c) Lognan. Red dots represent bedrock*
 395 *samples and green dots boulder samples. Outliers, rejected based on χ^2 statistics, are in italic*
 396 *grey font. Errors of individual ages correspond to the analytical error only. Mean ages are*
 397 *arithmetic means and standard deviation.*

398 In the *Lognan* area, the three bedrock samples taken from roches moutonnées slope between
 399 Rognons glacier and Argentière glacier yield ages of 11.0 ± 0.4 (ARG-15-7), 12.5 ± 0.5
 400 (ARG-15-6) and 11.0 ± 0.4 ka (ARG-15-5). From the moraine sequence located directly to
 401 the north, we dated three moraines (L1-L3), two of which lie very close together (L2, L3;
 402 Figure 7) The outmost one (L1) yields five boulder ages between 12.2 ± 0.6 and 10.6 ± 0.4
 403 ka, with a mean of 11.7 ± 0.7 ka, after discarding ARG-16-10 (10.1 ± 0.6 ka) as an outlier.
 404 Three boulders were dated from L2, giving ages between 10.3 ± 0.7 and 10.7 ± 0.3 ka and a
 405 mean age of 10.4 ± 0.2 ka. L3 yields five ages between 10.0 ± 0.3 and 10.9 ± 0.3 ka with a
 406 mean age of 10.4 ± 0.4 ka, after removing ARG-16-5 (17.4 ± 1.5 ka) as an outlier. These

407 glacial landform ages are in good stratigraphic order. The similar ^{10}Be ages of the latero-
 408 frontal moraines in the *La Joux* area (between ~ 10.9 ka and 9.7 ka) and of the lateral moraines
 409 in the Lognan area (between ~ 11.7 ka and 10.4 ka) implies that the deposition of these
 410 moraines most likely corresponds to the same glacier advances or stillstands.



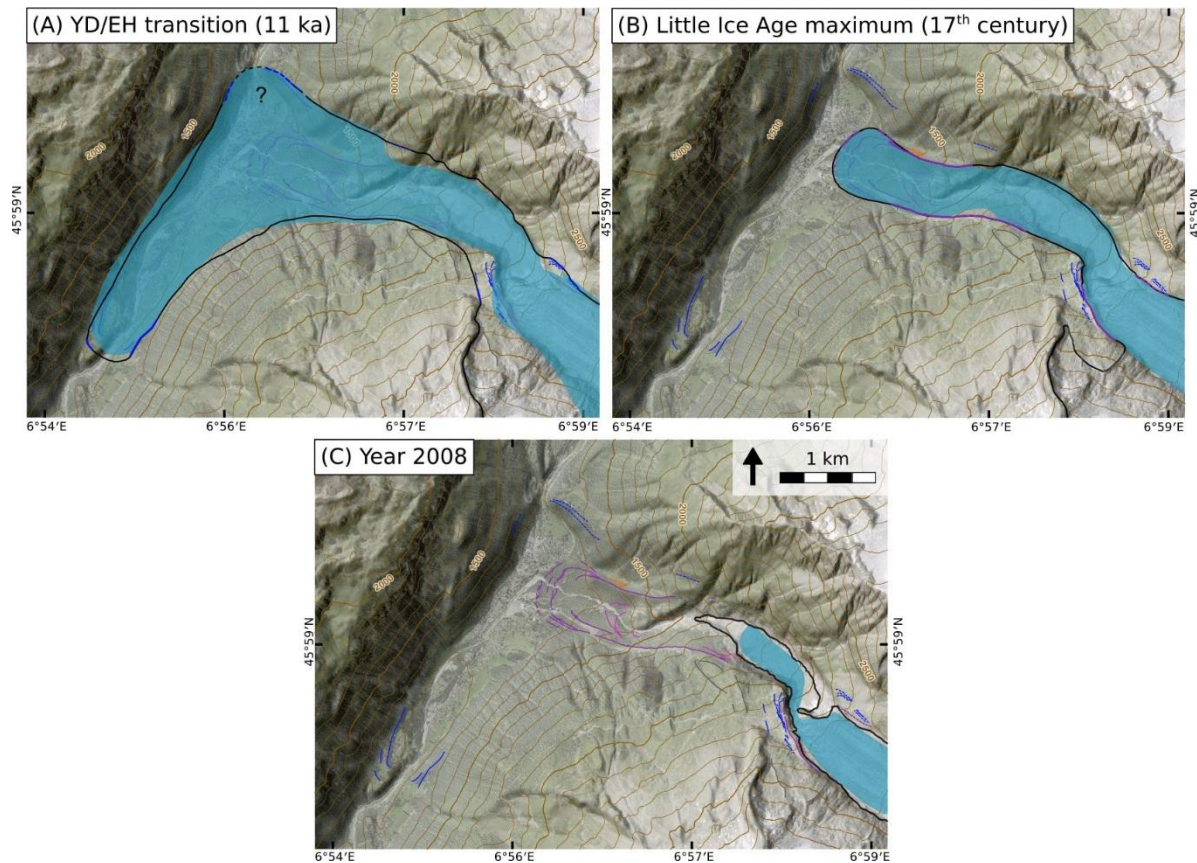
411
 412 *Figure 8 : Summed probability plots (colored curves – colors refer to the legend of Figure 2)*
 413 *of ^{10}Be boulder ages from Argentière glacier. Probability curves of individual ages (black*
 414 *curves) include analytical errors only. Ages indicated in each box are arithmetic means and*
 415 *standard deviations, also visually represented as vertical lines and colored band. Grey curves*
 416 *are outliers.*

417 Two additional bedrock surfaces were sampled next to the Lognan moraines. One on the foot
 418 of the bedrock slope at the southern extremity of L1 was dated at 10.4 ± 0.5 ka (ARG-16-8),
 419 and another one located between L1 and L3, taken from the flat ground, was dated at $10.0 \pm$
 420 0.4 ka (ARG-16-14). Even if these two ages are statistically indistinguishable from the mean

421 ages of the moraines that framed them and the low number of bedrock ages does not allow a
422 robust comparison, they apparently tend to be slightly younger than the moraines. This could
423 be explained by degradation and erosion of the samples (in the case of ARG-16-8) and
424 sediment, vegetation and/or snow cover, in particular for ARG-16-14 as it is on ground level,
425 which in both cases results in an underestimation of the ages.

426 The batch of the five samples taken in the *Crèmerie* area (C1 and C2 moraines) was subject to
427 a failure during the chemical preparation of the samples, leading to low-quality
428 measurements. Only sample ARG-17-2 from moraine C1 was retained due to sufficiently
429 high ^9Be currents ($>1 \mu\text{A}$) during the AMS measurements, and yielded an age of $0.9 \pm 0.2 \text{ ka}$.
430 However, as this is only a single moraine age with high analytical error and therefore does not
431 allow us to reliably interpret the deposition age of the moraines in the *Crèmerie* area, we do
432 not consider it further.

433 Based on presented ages and on the mapping of all preserved moraines, we reconstruct the
434 extents of the glacier during the YD/EH transition and the Little Ice Age maximum in
435 comparison with that of the year 2008, as shown in Figure 9.



436

437 *Figure 9 : Black curves represent the reconstruction of past extents of the Argentière glacier,*
 438 *based on mapping of the preserved moraines and interpretation of ^{10}Be dating, for the (A)*
 439 *Younger Dryas/Early Holocene transition (~ 11 ka - J2 moraines) (B) LIA maximum (17th*
 440 *century) and (C) year 2008. Dashed glacier limits with “?” correspond to hypothetical*
 441 *extents. Blue extensions represent the vertical projection of the 3D reconstruction with the*
 442 *ArcGIS toolbox GlaRe.*

443 **4.3. ELA determination**

444 The ELAs resulting from the different methods described in section 3.2 are presented in Table
 445 2. The contours of the ice surface resulting from the 3D reconstructions using the ArcGIS
 446 toolbox GlaRe and used for the ELAs calculations are represented in Figure 9 (blue areas).

447 According to the GIS-based reconstruction method, the ELAs computed for the glacier extent
 448 corresponding to the LIA maximum (17th century) and the moraine J2 (~ 11 ka) using the
 449 AABR method are 2738 m and 2523 m a.s.l., respectively. With the AAR method, they are

450 2753 m and 2648 m a.s.l., respectively. The ELA rise between the two extents is of 215 m
 451 with the AABR method, while it is 105 m with the AAR method. The modeling of the same
 452 extents using the PDD model, assuming the same precipitation as today, leads to ELA values
 453 of 2753 m for the 17th century and 2442 m a.s.l. for the ~11 ka period. The associated ELA
 454 rise between the two extents is 311 m.

	ELA (m a.s.l.)			Δ ELA (m)		
	present	LIA	~11 ka (J2 moraine)	LIA - present	~11 ka - present	11 ka - LIA
AABR	2866	2738	2523	128	343	215
AAR	2801	2753	2648	48	153	105
PDD	2940	2753	2442	187	498	311

455 *Table 2: Comparison of ELA calculations using the AABR and AAR methods and the PDD*
 456 *modeling for Argentière glacier for the present-day (i.e. year 2008 for the AABR and AAR*
 457 *methods and 1979-2002 for the PDD modeling), the LIA maximum (17th century) and the J2*
 458 *moraine (~11 ka; YD/EH transition). For the AABR method a Balance ratio of 1.59 (Rea,*
 459 *2009) is used and for the AAR method a ratio of 0.67 (Gross et al., 1977), both representative*
 460 *for the Alps. For the PDD model, ELA values are inferred with the same precipitation*
 461 *condition as today.*

462 **4.4. Paleoclimatic results**

463 *4.4.1. Temperature results from the GIS-based reconstructions*

464 The temperature differences inferred from the GIS-based ELA reconstructions (AABR and
 465 AAR methods) between ~11 ka, the LIA maximum (17th century) and the year 2008 are
 466 presented in Table 3. The 128-m rise of the ELA between the LIA maximum and the year
 467 2008 inferred from the AABR method is equivalent to a +1.1°C difference in summer
 468 temperature, according to the ELA sensitivity to summer temperature of 115 m°C⁻¹ (Rabatel
 469 et al., 2013). Using the local ELA sensitivity of 72 m°C⁻¹ (Six and Vincent, 2014), it is
 470 +1.8°C. The temperature difference between ~11 ka and the year 2008 (ELA-rise of 331 m),

471 using the same two ELA temperature-sensitivity values as above, is +3°C and +4.8°C,
 472 respectively.

473 For the sake of comparison with other studies from the Alps, we also give the results from the
 474 AAR method, noting that the ELA-rise is traditionally estimated with reference to the LIA
 475 maximum glacier extent. According to this approach, our reconstruction leads to an ELA-rise
 476 between ~11 ka and the LIA maximum of 105 m, which corresponds to +0.9°C and +1.4°C,
 477 respectively. Between ~11 ka and 2008, this approach gives a difference of +1.3°C and
 478 +2.1°C, respectively, equivalent to an ELA rise of 153 m. And between the LIA maximum
 479 and 2008, the ELA-rise is 48 m, corresponding to a temperature difference of +0.4°C and
 480 +0.7°C, respectively. These latter results seem to be underestimated when comparing them to
 481 the values inferred from the measurements at the beginning of the 19th century (~+1.0°C;
 482 Auer et al., 2007; Figure 5), a period when the glacier was even slightly smaller than during
 483 the 17th century. On the other hand, the temperature results from the AABR method
 484 (+1.1°C/+1.8°C) are coherent with the instrumental data.

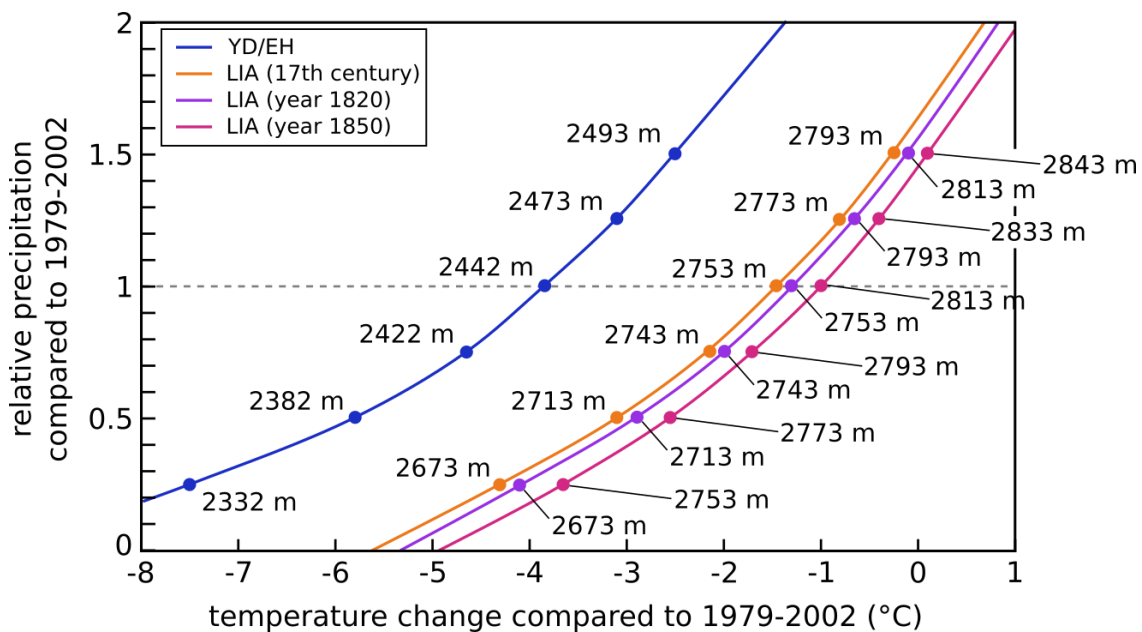
	ΔT [LIA - year 2008] (°C)		ΔT [~11 ka - year 2008] (°C)		ΔT [~11 ka - LIA] (°C)	
AABR	+1.1	+1.8	+3.0	+4.8	+1.8	+2.9
AAR	+0.4	+0.7	+1.3	+2.1	+0.9	+1.4

485 *Table 3: Comparison of the temperature differences inferred from the ΔELA calculated from*
 486 *the AABR and AAR methods (presented in Table 2) using two different ELA sensitivity to*
 487 *temperature: 115 m°C⁻¹ (Rabatel et al., 2013) on the left and 72 m°C⁻¹ (Six and Vincent,*
 488 *2014) on the right. LIA refers to the LIA maximum (17th century).*

489 4.4.2. Paleoclimatic results from the PDD modeling

490 Applying the PDD modeling approach, we determined the potential combinations of
 491 precipitation and temperature conditions corresponding to each investigated glacier extent.
 492 The glacier extents at four different dates were investigated (see Figure 2 to visualize the
 493 extents): the years 1850 and 1820, for which the glacier extents and regional climate

494 conditions are well known, the 17th century (LIA maximum) and the extent at ~11 ka using
 495 the moraine J2 as the frontal limit. The modeling gives an infinite number of combinations of
 496 temperature and precipitation conditions that explain the frontal moraine position at the four
 497 investigated dates. The curves in Figure 10 represent these combinations, considering
 498 temperatures between 0°C and 8°C below that of the reference period (1979-2002) and
 499 precipitation amounts between 0 and 2 times that of the reference period. This figure also
 500 shows the range of ELAs resulting from the model for each of the four glacier extents. The
 501 ELAs increase with precipitation.

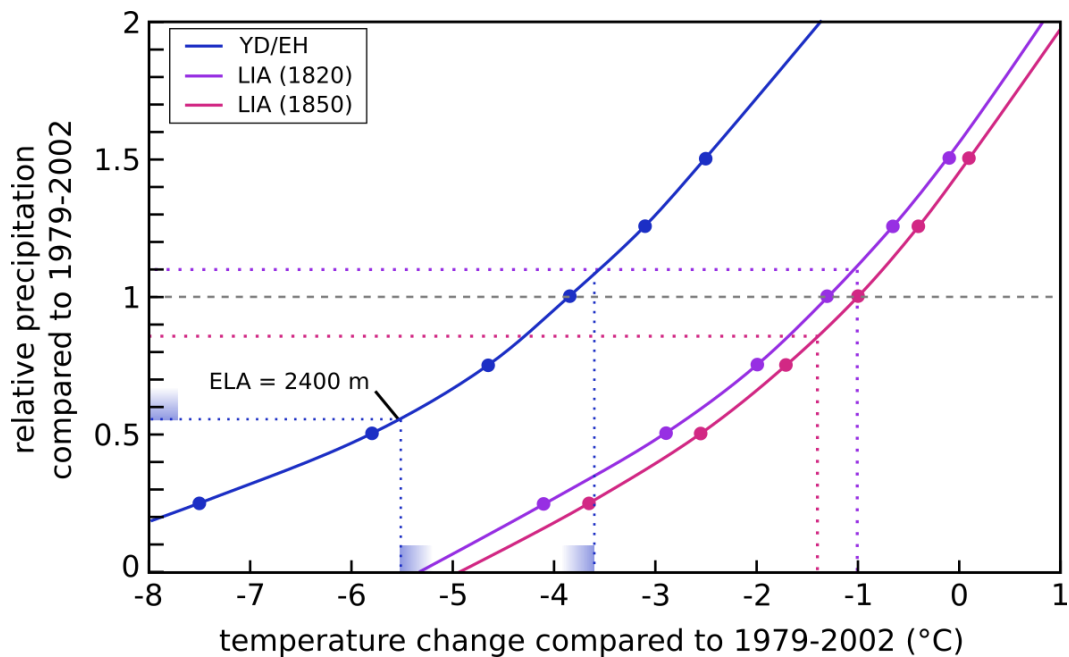


502
 503 *Figure 10 : Paleoclimatic reconstructions of the Argentière glacier for the YD/EH transition*
 504 *(blue) and the 17th century (orange), 1820 (purple) and 1850. (pink) glacier extent.*
 505 *Temperature changes, with respect to the 1979-2002 period, are plotted against relative*
 506 *precipitation amount normalized to the 1979-2002 period. One curve reflects all*
 507 *combinations of temperature and precipitation for one glacier extent (constrained by the*
 508 *frontal moraines). The altitudes refer to the ELA associated with each temperature-*
 509 *precipitation couple.*

510 Climate influence on Argentière glacier is explored through modeling of its extents at the end
511 of the LIA, when climatic evolution is already instrumentally recorded. As the instrumental
512 climatic data used for comparison with our results do not cover the 17th century, only the
513 results of 1850 and 1820 are subject to discussions of the LIA paleoclimate. Based on the data
514 collected in the HISTALP project (<http://www.zamg.ac.at/histalp/>; Auer et al., 2007), we
515 estimate the annual temperature for the years 1850 and 1820. We then deduce the
516 precipitation, which is more likely to vary locally, from the PDD model. All values are
517 calculated relative to the 1979-2002 period, which is the “present-day” reference period used
518 in the PDD model (see section 3.2). A shift of 10-14 years between the extraction of the
519 temperature value and the date of the studied extent has been applied in order to take into
520 account the glacier’s response time (Vincent et al., 2009). The measured temperature
521 differences compared to the period of reference are around -1.4°C for 1850 and around -1.0°C
522 for 1820 (Figure 5). Thus, colder conditions prevailed when the glacier was shorter, in 1850.
523 According to these temperature differences and the temperature-precipitation relationships in
524 Figure 11, precipitation amounts were lower by ~15% in 1850 and higher by ~10% in 1820
525 compared to the 1979-2002 average. If the temperatures had been inferred from our PDD
526 model assuming the same amount of precipitation as in 1979-2002, the 1850 temperature
527 would have been overestimated by ~0.4°C and the 1820 temperature underestimated by
528 ~0.2°C.

529 Constraining a unique temperature/precipitation couple for the ~11 ka glacier extent is much
530 more challenging due to the scarcity and uncertainties of pure paleo-precipitation and paleo-
531 temperature records for this time in the Alps. Therefore, we use the following rationales to
532 narrow down the potential range of precipitation/temperature couples. As moraines are only
533 built below the ELA (e.g. Anderson and Anderson, 2010) and the maximal elevation of the
534 moraine sequence corresponding to the YD/EH transition on the glacier bank opposite to the

535 Lognan area is ~2400 m a.s.l. (Figure 2), the ELA during this period was at least as high as
 536 2400 m. This observation allows us to limit the temperature difference compared to 1979-
 537 2002 to -5.5°C (lower bound) and to a minimum of 45% of the 1979-2002 averaged
 538 precipitation amount (Figure 10 and Figure 11). Then, assuming that the amount of
 539 precipitation was not superior to that during the end of the LIA, i.e. up to 10% precipitation
 540 more than during the 1979-2002 period, the upper temperature limit is at -3.6°C . The
 541 temperature values of -3°C and -4.8°C , inferred above from the GIS based estimations
 542 (AABR method) for the same glacier extent, compare well with these temperature bounds of -
 543 5.5°C and -3.6°C resulting from the PDD model, supporting the findings from both methods.
 544 The relatively high potential temperature ranges reflect the uncertainty arising from the choice
 545 of the value for the ELA sensitivity to temperature in the first approach and from the range of
 546 possible precipitation amounts in the second approach.



547
 548 *Figure 11 : Same as Fig. 10, but for the YD/EH transition (blue), 1820 (purple) and 1850*
 549 *(pink) glacier extent only, with marks of the paleoclimatic interpretations.*

550

551 **5 Discussion**

552 **5.1. Holocene oscillations of Argentière glacier**

553 As outlined in section 2, numerous glacio-geomorphic markers in the Arve valley attest to the
554 glacier extents during the LGM and to various advances or stillstands during the deglaciation
555 of the Late-glacial. The moraine ages from the La Joux and Lognan areas are younger than
556 11.7 ka and therefore fall into the Early Holocene, apart from L1 moraine, which overlaps
557 with the Younger Dryas within uncertainties. The ^{10}Be ages of the three roche moutonnée
558 samples located between Rognons and Argentière glacier (11.0 ± 0.4 ka, 12.5 ± 0.4 ka, $11.0 \pm$
559 0.4 ka) and of the Lognan bedrock surfaces (10.4 ± 0.5 ka and 10.0 ± 0.4 ka) suggest that the
560 general deglaciation of this area occurred during the YD/EH transition. These ages are
561 statistically the same as the ^{10}Be mean ages of moraines L1, L2 and L3 (11.7 ± 0.7 ka, $10.4 \pm$
562 0.2 ka and 10.4 ± 0.4 ka) in the Lognan area, indicating that the deglaciation process was
563 shortly interrupted by glacier stillstands or re-advances. The isolated bloc dated at 13.2 ± 0.4
564 ka in front of the J1 moraine in the *La Joux* area tentatively suggests that the front of the
565 glacier may already have retreated to a similar position as moraines J1 and J2 ~ 2 ka before the
566 YD/EH transition, but this scenario would need more evidence to be confirmed. The existence
567 of at least five morainic ridges between L1 and L3 (Figure 7C) indicate that Argentière
568 glacier stagnated or re-advanced at least five times between ~ 11.7 and ~ 10.4 ka ago. These
569 results from the lateral moraines in the Lognan area are coherent with the observations in the
570 frontal area of *La Joux*, where at least three preserved ridges of Early Holocene age (~ 11 ka)
571 can be distinguished (among them J1 and J2). The similarity of the moraine and bedrock ages
572 as well as the smooth and low morphology of the moraines suggest that the glacier did not
573 retreat far up-valley between the moments of moraine deposition and that these moraines
574 correspond to periods of glacier stillstands during the deglaciation rather than to massive re-
575 advances. Finally, the innermost moraine ages and the bedrock ages in the Lognan area imply
576 that the glacier definitively retreated from its Early Holocene extent at ~ 10.4 ka ago.

577 Further evidence of advanced extents of Argentière glacier during the Late Holocene comes
578 from the study by Bless (1984) who suggested five advances of Argentière glacier between ~4
579 ka and ~1.2 ka, based on radiocarbon-dated subfossil wood found in the right-lateral moraine
580 outcrop (location in Figure 2). Multiple advances during this period were also reported for
581 other glaciers in the Mont-Blanc massif (e.g. Deline and Orombelli, 2005; Le Roy et al.,
582 2015). In particular, the numerous dendrochronologically-dated advances of the neighbor Mer
583 de Glace between ~3.5 ka and 0.7 ka ago (Le Roy et al. (2015); location in Figure 1), support
584 the hypothesis of Late Holocene advances of Argentière glacier. However, considering that so
585 far none of the preserved and dated moraines gave a Late Holocene age that pre-dates the
586 LIA, we assume that the Late Holocene extents of Argentière glacier were smaller than those
587 during the LIA maximum.

588 **5.2. Paleoclimatic interpretations**

589 *5.2.1. Comparison with previously glacier-derived paleoclimate reconstructions from* 590 *Argentière glacier and other sites in the Alps*

591 The results of the PDD modeling for the 1820 and 1850 extents indicate that precipitation was
592 higher in 1820 than in 1850. Regionally higher precipitation in 1820 was also recorded in the
593 western part of the Alps according to the HISTALP annual precipitation time series (Figure
594 5), but the difference in precipitation amount between 1850 and 1820 is only of ~10%, against
595 ~20% according to our modeling. Our results are consistent with the conclusions from
596 previous PDD modeling of Argentière glacier (Vincent et al., 2005), which explains observed
597 glacier advances during the period 1760-1830 with winter precipitations higher by at least
598 25% than the 20th century average, while summer temperature had not decreased. They also
599 attribute the subsequent retreat of the glacier to a decrease in winter precipitation. Even if our
600 findings are not directly comparable, as our modelling only allows us to consider the annual
601 and not the seasonal climate variations and Vincent et al. (2005) based their model on less

602 cooling than we do here, we can still notice that the trend is the same, i.e. higher precipitation
603 in 1820 compared to 1850 explains the bigger glacier extent. Given that the 19th century
604 maximum of bigger glaciers in the Swiss Alps occurred in 1850-1860 rather than in 1820
605 (Holzhauser et al., 2005), the glacier size and local variations in precipitations during the LIA
606 could explain the detailed differences in the behavior of Argentière glacier compared to
607 smaller glaciers in other Alpine regions. These results illustrate that ignoring the role of
608 precipitation might lead to a first-order approximation of past temperature conditions. Our
609 results also show that the impact of local precipitation variations on mountain glacier
610 dynamics superimposes on those of large scale temperature variations and can thus explain
611 the local differences in the behavior of glaciers from different parts of a massif, like the Alps,
612 and the small fluctuations of a glacier during one glacial stadial, like the LIA.

613 Temperature reconstructions for the YD/EH transition using the AAR method have
614 previously been performed at glacier sites in the Alps. Moran et al. (2016) reconstructed from
615 the extents of two glaciers in the Eastern Alps that summer temperatures were 1.5°C lower
616 during the YD/EH transition than in the mid 20th century, which is in good agreement with the
617 difference of 1.3°C/2.1°C inferred from the extents of Argentière glacier during the YD/EH
618 transition and the year 2008 when using the AAR method. These results are also coherent
619 with the findings of Hofmann et al. (2019) who inferred a temperature difference of 1.5°C
620 between the YD/EH transition and the LIA in the westernmost French Alps. Nonetheless, due
621 to the extremely simplified assumptions on the glacier geometry of the AAR method (section
622 3.3.1), we believe that temperature reconstructions based on this approach should be taken
623 with caution. The coherence between the relative temperature reconstructed from the local
624 LIA maximum glacier extent and the one measured at the end of the LIA (section 4.4.1)
625 makes us indeed confident that the AABR method is more reliable than the AAR method
626 when inferring paleotemperatures from ELA reconstructions.

627 5.2.2. Comparison with paleoclimate results from independent proxy records

628 Comparison of our precipitation range assumptions for the YD/EH transition (-45% to +10%
629 of the present precipitation amount) with independent proxy records is difficult. Given that
630 precipitation can significantly vary locally, it would be ideal to consider a local precipitation
631 estimate in or near the Mont-Blanc massif for this period. However, to our knowledge this
632 does not exist. The complexity of the precipitation variability during the Younger Dryas and
633 the Early Holocene has indeed been underlined by Magny et al. (2001). Recent global climate
634 simulations combined with proxy-based temperature reconstructions suggest that the Younger
635 Dryas was considerably drier and the Early Holocene was less dry in Central Europe than the
636 preceding Allerod period (Renssen et al., 2018), but no quantification of the precipitation
637 conditions relative to the present is available.

638 Alpine and European temperature reconstructions for the Younger Dryas and Early Holocene
639 based on independent proxies are more frequent. However, the range of reconstructed annual
640 and summer temperatures for the Younger Dryas is large, it varies from 6 to 2°C below
641 modern values when inferred from records of pollen and cladocera assemblages from
642 Gerzensee in the North-alpine foreland in Switzerland (Lotter et al., 2000), investigation of
643 stalagmites in Hölloch cave in the German Alps (Wurth et al., 2004) or chironomid records
644 from a paleolake in the Central Swiss Alps (Ilyashuk et al., 2009). Based on high-resolution
645 oxygen isotope records, the beginning of the Holocene is associated with an abrupt
646 temperature rise on regional and hemispheric scale (Alley, 2000; Schwander et al., 2000).
647 Early Holocene temperature reconstructions in the region of the Alps yield, similar to those
648 for the Younger Dryas, a large range of values depending on the used proxy. For example, the
649 chironomid record in the Swiss central Alps indicates ~1-4°C *above* the present July air
650 temperatures for the very beginning of the Holocene (Ilyashuk et al., 2009), while a second
651 chironomid record, also from the Swiss Alps, indicates ~1-1.5°C *below* it (Heiri et al., 2003).

652 Reconstruction from pollen data indicates an annual anomaly relative to the present of as low
653 as -4.5°C (around 12-11 ka) for the central-western part of Europe (Davis et al., 2003) and
654 summer temperatures of $4.5\text{-}5^{\circ}\text{C}$ below those of the present at Gerzensee (Lotter et al., 2000).
655 The temperature range inferred for the YD/EH transition from our PDD modeling of -5.5°C to
656 -3.6°C and from the ELA reconstruction with the AABR method of $-4.8^{\circ}\text{C}/-3.0^{\circ}\text{C}$, agrees
657 with the coldest results from alpine proxy records for this period (e.g. Davis et al., 2003;
658 Lotter et al., 2000), reinforcing our results for the western Alps.
659 However, the large divergence between the paleo-temperature reconstructions depending on
660 the method and parameters used highlights that further investigations are necessary to refine
661 methods that aim at inferring paleo-climate conditions from past glacier extents and to
662 complete the here presented findings.

663

664 **6. Conclusions**

665 Our new Holocene chronology for the Argentière glacier based on 29 cosmogenic ^{10}Be
666 cosmogenic dates of moraines and bedrock suggests that Argentière glacier retreated from its
667 large Late-Glacial extent during the Younger Dryas/Early Holocene transition, around 11.7
668 ka, and that this retreat was interrupted by several stillstands during ~ 1 ka, followed at ~ 10.4
669 by the final glacier retreat to within the LIA limits. We do not have any evidence of glacial
670 advances until the Late Holocene.

671 Climate reconstruction corresponding to two different glacier extents during the LIA, using a
672 PDD model coupled with a dynamic ice flow model, highlights the influence of local
673 precipitation changes, superimposed on the dominant impact of temperature, on the detailed
674 glacial fluctuations of Argentière glacier. This suggests that disregarding the role of
675 precipitation might lead to first-order temperature approximations when reconstruction paleo-
676 climate conditions from past glacier extents.

677 The reconstruction of the climatic conditions corresponding to the YD/EH transition extent of
678 the glacier using the PDD model and a simpler approach that only considers the impact of
679 summer temperature on the reconstructed ELAs yield comparable results. The results from
680 the PDD model suggests a temperature difference range of -5.5°C to -3.6°C compared to the
681 present-day period (1979-2002). This agrees with earlier paleoclimate reconstructions from
682 pollen records for the same period, but seems to be quite cold in comparison with the results
683 from other proxy studies and another simple approach of glacier-based temperature
684 reconstruction. The large differences in temperature reconstructions from the various
685 paleoclimate studies and the scarcity of paleo-precipitation records for the Younger Dryas and
686 the Early Holocene highlight the need of additional efforts in investigating the paleoclimatic
687 conditions for these periods.

688

689 **Acknowledgements**

690 This study is part of ANR project 14-CE03-0006 *VIP Mont-Blanc*. We thank Laëtitia Léanni
691 (CEREGE) for support during sample chemistry, Pierre Jégot and Jules Fleury (CEREGE) for
692 help during ELA determination and Daniel Joly and Benjamin Pohl for sharing temperature
693 and precipitation data. The 2015 DEM of Argentière glacier catchment has been acquired
694 within the project ISOTHERM led by Antoine Rabatel (Univ. Grenoble Alpes, IGE) founded
695 by EUFAR (EUropean Facility for Airborne Research). We also thank the IRSTEA for the
696 Arve valley DEM. The ASTER AMS national facility (CEREGE) is supported by the
697 INSU/CNRS, the ANR through the “projet thématiques d’excellence” program for the
698 “Equipements d’excellence” ASTER-CEREGE action and IRD. We thank Benjamin
699 Chandler and one anonymous reviewer whose relevant remarks have helped to improve this
700 manuscript.

701

702 **References**

- 703 Alley, R.B., 2000. The Younger Dryas cold interval as viewed from central Greenland. *Quat.*
704 *Sci. Rev.* 19, 213–226. [https://doi.org/10.1016/S0277-3791\(99\)00062-1](https://doi.org/10.1016/S0277-3791(99)00062-1)
- 705 Anderson, R.S., Anderson, S.P., 2010. *Geomorphology: The Mechanics and Chemistry of*
706 *Landscapes*. 2010. Cambridge University Press, 340 pp.
- 707 André, M., 2002. Rates of postglacial rock weathering on glacially scoured outcrops (abisko–
708 riksgården area, 68°N). *Geogr. Ann. Ser. Phys. Geogr.* 84, 139–150.
709 <https://doi.org/10.1111/j.0435-3676.2002.00168.x>
- 710 Arnold, M., Merchel, S., Bourlès, D.L., Braucher, R., Benedetti, L., Finkel, R.C., Aumaître,
711 G., Gottang, A., Klein, M., 2010. The French accelerator mass spectrometry facility ASTER:
712 Improved performance and developments. *Nucl. Instrum. Methods Phys. Res. Sect. B Beam*
713 *Interact. Mater. At.*, 19th International Conference on Ion Beam Analysis 268, 1954–1959.
714 <https://doi.org/10.1016/j.nimb.2010.02.107>
- 715 Auer, I., Böhm, R., Jurkovic, A., Lipa, W., Orlik, A., Potzmann, R., Schöner, W.,
716 Ungersböck, M., Matulla, C., Briffa, K., Jones, P., Efthymiadis, D., Brunetti, M., Nanni, T.,
717 Maugeri, M., Mercalli, L., Mestre, O., Moisselin, J.-M., Begert, M., Müller-Westermeier, G.,
718 Kveton, V., Bochnicek, O., Stastny, P., Lapin, M., Szalai, S., Szentimrey, T., Cegnar, T.,
719 Dolinar, M., Gajic-Capka, M., Zaninovic, K., Majstorovic, Z., Nieplova, E., 2007.
720 HISTALP—historical instrumental climatological surface time series of the Greater Alpine
721 Region. *Int. J. Climatol.* 27, 17–46. <https://doi.org/10.1002/joc.1377>
- 722 Balco, G., Briner, J., Finkel, R.C., Rayburn, J.A., Ridge, J.C., Schaefer, J.M., 2009. Regional
723 beryllium-10 production rate calibration for late-glacial northeastern North America. *Quat.*
724 *Geochronol.* 4, 93–107. <https://doi.org/10.1016/j.quageo.2008.09.001>
- 725 Baroni, C., Casale, S., Salvatore, M.C., Ivy-Ochs, S., Christl, M., Carturan, L., Seppi, R.,
726 Carton, A., 2017. Double response of glaciers in the Upper Peio Valley (Rhaetian Alps, Italy)
727 to the Younger Dryas climatic deterioration. *Boreas* 46, 783–798.
728 <https://doi.org/10.1111/bor.12284>
- 729 Benn, D.I., Lehmkuhl, F., 2000. Mass balance and equilibrium-line altitudes of glaciers in
730 high-mountain environments. *Quat. Int.* 65–66, 15–29. [https://doi.org/10.1016/S1040-](https://doi.org/10.1016/S1040-6182(99)00034-8)
731 [6182\(99\)00034-8](https://doi.org/10.1016/S1040-6182(99)00034-8)
- 732 Biette, M., Jomelli, V., Favier, V., Chenet, M., Agosta, C., Fettweis, X., Minh, D.H.T., Ose,
733 K., 2018. Estimation des températures au début du dernier millénaire dans l’ouest du
734 Groenland : résultats préliminaires issus de l’application d’un modèle glaciologique de type

735 degré-jour sur le glacier du Lyngmarksbræen. *Géomorphologie Relief Process. Environ.* 24.
736 <https://doi.org/10.4000/geomorphologie.11977>

737 Blard, P.-H., Lavé, J., Pik, R., Wagnon, P., Bourlès, D., 2007. Persistence of full glacial
738 conditions in the central Pacific until 15,000 years ago. *Nature* 449, 591–594.
739 <https://doi.org/10.1038/nature06142>

740 Bless, R., 1984. Beiträge zur Spät und Postglazialen Geschichte der Gletscher im
741 Nordöstlichen Mont Blanc Gebiet. *Phys. Geogr.* 15.

742 Braucher, R., Guillou, V., Bourlès, D.L., Arnold, M., Aumaître, G., Keddadouche, K.,
743 Nottoli, E., 2015. Preparation of ASTER in-house $^{10}\text{Be}/^{9}\text{Be}$ standard solutions. *Nucl.*
744 *Instrum. Methods Phys. Res. Sect. B Beam Interact. Mater. At.*, The Thirteenth Accelerator
745 Mass Spectrometry Conference 361, 335–340. <https://doi.org/10.1016/j.nimb.2015.06.012>

746 Bussy, F., Hernandez, J., Raumer, J.V., 2000. Bimodal magmatism as a consequence of the
747 post-collisional readjustment of the thickened Variscan continental lithosphere (Aiguilles
748 Rouges-Mont Blanc Massifs, Western Alps). *Earth Environ. Sci. Trans. R. Soc. Edinb.* 91,
749 221–233. <https://doi.org/10.1017/S0263593300007392>

750 Chenet, M., Brunstein, D., Jomelli, V., Roussel, E., Rinterknecht, V., Mokadem, F., Biette,
751 M., Robert, V., Léanni, L., 2016. ^{10}Be cosmic-ray exposure dating of moraines and rock
752 avalanches in the Upper Romanche valley (French Alps): Evidence of two glacial advances
753 during the Late Glacial/Holocene transition. *Quat. Sci. Rev.* 148, 209–221.
754 <https://doi.org/10.1016/j.quascirev.2016.07.025>

755 Chmeleff, J., von Blanckenburg, F., Kossert, K., Jakob, D., 2010. Determination of the ^{10}Be
756 half-life by multicollector ICP-MS and liquid scintillation counting. *Nucl. Instrum. Methods*
757 *Phys. Res. Sect. B Beam Interact. Mater. At.* 268, 192–199.
758 <https://doi.org/10.1016/j.nimb.2009.09.012>

759 Claude, A., Ivy-Ochs, S., Kober, F., Antognini, M., Salcher, B., Kubik, P.W., 2014. The
760 Chironico landslide (Valle Leventina, southern Swiss Alps): age and evolution. *Swiss J.*
761 *Geosci.* 107, 273–291. <https://doi.org/10.1007/s00015-014-0170-z>

762 Corbel, J., 1963. Glaciers et climats dans le massif du Mont-Blanc. *Rev. Géographie Alp.* 51,
763 321–360. <https://doi.org/10.3406/rga.1963.3132>

764 Coutterand, S., Buoncristiani, J.-F., 2006. Paléogéographie du dernier maximum glaciaire du
765 Pléistocène récent de la région du Massif du Mont Blanc, France. *Quat. Rev. Assoc. Fr. Pour*
766 *L'étude Quat.* 35–43. <https://doi.org/10.4000/quatenaire.633>

767 Coutterand, S., Nicoud, G., 2005. Les stades de retrait du glacier de l'Arve entre le verrou de
768 cluses et l'ombilic de Chamonix au cours du Tardiglaciaire (Vallée de l'Arve, Haute-Savoie).

769 Quaternaire 85–94. <https://doi.org/10.4000/quaternaire.296>

770 Davis, B.A.S., Brewer, S., Stevenson, A.C., Guiot, J., 2003. The temperature of Europe
771 during the Holocene reconstructed from pollen data. *Quat. Sci. Rev.* 22, 1701–1716.
772 [https://doi.org/10.1016/S0277-3791\(03\)00173-2](https://doi.org/10.1016/S0277-3791(03)00173-2)

773 Deline, P., Orombelli, G., 2005. Glacier fluctuations in the western Alps during the
774 Neoglacial, as indicated by the Miage morainic amphitheatre (Mont Blanc massif, Italy).
775 *Boreas* 34, 456–467. <https://doi.org/10.1080/03009480500231369>

776 Fischer, M., Huss, M., Barboux, C., Hoelzle, M., 2014. The New Swiss Glacier Inventory
777 SGI2010: Relevance of Using High-Resolution Source Data in Areas Dominated by Very
778 Small Glaciers. *Arct. Antarct. Alp. Res.* 46, 933–945. [https://doi.org/10.1657/1938-4246-](https://doi.org/10.1657/1938-4246-46.4.933)
779 [46.4.933](https://doi.org/10.1657/1938-4246-46.4.933)

780 Fontaine, R., 2015. Chamonix et ses glaciers : Les premières images sous l’œil des
781 photographes (1849-1869), Atelier Esope. ed.

782 Francou, B., Vincent, C., 2007. Les glaciers à l’épreuve du climat, Edition IRD. ed.

783 Gardent, M., Rabatel, A., Dedieu, J.-P., Deline, P., 2014. Multitemporal glacier inventory of
784 the French Alps from the late 1960s to the late 2000s. *Glob. Planet. Change* 120, 24–37.
785 <https://doi.org/10.1016/j.gloplacha.2014.05.004>

786 Gross, G., Kerschner, H., Patzelt, G., 1977. Methodische Untersuchungen über
787 die Schneegrenze in alpinen Gletschergebieten. *Gletsch Glazialgeol* 223–251.

788 Heiri, O., Lotter, A.F., Hausmann, S., Kienast, F., 2003. A chironomid-based Holocene
789 summer air temperature reconstruction from the Swiss Alps. *The Holocene* 13,
790 477–484. <https://doi.org/10.1191/0959683603hl640ft>

791 Hofmann, F.M., Alexanderson, H., Schoeneich, P., Mertes, J.R., Léanni, L., Aster Team
792 (Georges Aumaître, Didier L. Bourlès, Karim Keddadouche), 2019. Post-Last Glacial
793 Maximum glacier fluctuations in the southern Écrins massif (westernmost Alps): insights
794 from ¹⁰Be cosmic ray exposure dating. *Boreas*. <https://doi.org/10.1111/bor.12405>

795 Holzhauser, H., Magny, M., Zumbühl, H.J., 2005. Glacier and lake-level variations in west-
796 central Europe over the last 3500 years. *The Holocene* 15, 789–801.
797 <https://doi.org/10.1191/0959683605hl853ra>

798 Ilyashuk, B., Gobet, E., Heiri, O., Lotter, A.F., van Leeuwen, J.F.N., van der Knaap, W.O.,
799 Ilyashuk, E., Oberli, F., Ammann, B., 2009. Lateglacial environmental and climatic changes
800 at the Maloja Pass, Central Swiss Alps, as recorded by chironomids and pollen. *Quat. Sci.*
801 *Rev.* 28, 1340–1353. <https://doi.org/10.1016/j.quascirev.2009.01.007>

802 Jaillet, S., Ballandras, S., 1999. La transition Tardiglaciaire/Holocène à travers les

803 fluctuations du glacier du Tour (Vallée de Chamonix, Alpes du Nord françaises)
804 [Lateglacial/Holocene transition through glacier du Tour fluctuations (upper Chamonix
805 valley, French Alps)]. *Quaternaire* 10, 15–23. <https://doi.org/10.3406/quate.1999.1625>

806 Joly, D., Berger, A., Buoncristiani, J.-F., Champagne, O., Pergaud, J., Richard, Y., Soare, P.,
807 Pohl, B., 2018. Geomatic downscaling of temperatures in the Mont Blanc massif: A NEW
808 STATISTICAL DOWNSCALING APPROACH. *Int. J. Climatol.* 38, 1846–1863.
809 <https://doi.org/10.1002/joc.5300>

810 Jomelli, V., Khodri, M., Favier, V., Brunstein, D., Ledru, M.-P., Wagnon, P., Blard, P.-H.,
811 Sicart, J.-E., Braucher, R., Grancher, D., Bourlès, D.L., Braconnot, P., Vuille, M., 2011.
812 Irregular tropical glacier retreat over the Holocene epoch driven by progressive warming.
813 *Nature* 474, 196–199. <https://doi.org/10.1038/nature10150>

814 Keeler, D.G., 2015. Development and Validation of a Physically Based ELA Model and its
815 Application to the Younger Dryas Event in the Graubünden Alps, Switzerland 70.

816 Kerschner, H., Ivy-Ochs, S., 2007. Palaeoclimate from glaciers: Examples from the Eastern
817 Alps during the Alpine Lateglacial and early Holocene. *Glob. Planet. Change* 60, 58–71.
818 <https://doi.org/10.1016/j.gloplacha.2006.07.034>

819 Korschinek, G., Bergmaier, A., Faestermann, T., Gerstmann, U.C., Knie, K., Rugel, G.,
820 Wallner, A., Dillmann, I., Dollinger, G., von Gostomski, Ch.L., Kossert, K., Maiti, M.,
821 Poutivtsev, M., Remmert, A., 2010. A new value for the half-life of ^{10}Be by Heavy-Ion
822 Elastic Recoil Detection and liquid scintillation counting. *Nucl. Instrum. Methods Phys. Res.*
823 *Sect. B Beam Interact. Mater. At.* 268, 187–191. <https://doi.org/10.1016/j.nimb.2009.09.020>

824 Le Roy, M., 2012. Reconstitution des fluctuations glaciaires holocènes dans les Alpes
825 occidentales : apports de la dendrochronologie et de la datation par isotopes cosmogéniques
826 produits in situ (phdthesis). Université Grenoble Alpes.

827 Le Roy, M., Deline, P., Carcaillet, J., Schimmelpfennig, I., Ermini, M., 2017. ^{10}Be exposure
828 dating of the timing of Neoglacial glacier advances in the Ecrins-Pelvoux massif, southern
829 French Alps. *Quat. Sci. Rev.* 178, 118–138. <https://doi.org/10.1016/j.quascirev.2017.10.010>

830 Le Roy, M., Nicolussi, K., Deline, P., Astrade, L., Edouard, J.-L., Miramont, C., Arnaud, F.,
831 2015. Calendar-dated glacier variations in the western European Alps during the Neoglacial:
832 the Mer de Glace record, Mont Blanc massif. *Quat. Sci. Rev.* 108, 1–22.
833 <https://doi.org/10.1016/j.quascirev.2014.10.033>

834 Leclercq, P.W., Oerlemans, J., Basagic, H.J., Bushueva, I., Cook, A.J., Le Bris, R., 2014. A
835 data set of worldwide glacier length fluctuations. *The Cryosphere* 8, 659–672.
836 <https://doi.org/10.5194/tc-8-659-2014>

837 Lotter, A.F., Birks, H.J.B., Eicher, U., Hofmann, W., Schwander, J., Wick, L., 2000. Younger
838 Dryas and Allerød summer temperatures at Gerzensee (Switzerland) inferred from fossil
839 pollen and cladoceran assemblages. *Palaeogeogr. Palaeoclimatol. Palaeoecol.* 159, 349–361.
840 [https://doi.org/10.1016/S0031-0182\(00\)00093-6](https://doi.org/10.1016/S0031-0182(00)00093-6)

841 Lucéna, S., Ballandras, S., 1999. Rythme des fluctuations glaciaires et détritisme alluvial
842 postglaciaire dans la haute vallée de l'Arve (Alpes françaises du Nord) [Glacial fluctuations
843 rhythm and postglacial alluvial detritism in high Arve valley (French North Alps)]. *Quaternaire*
844 10, 25–36. <https://doi.org/10.3406/quate.1999.1626>

845 Lukas, S., 2007. Early-Holocene glacier fluctuations in Krundalen, south central Norway:
846 palaeoglacier dynamics and palaeoclimate. *The Holocene* 17, 585–598.
847 <https://doi.org/10.1177/0959683607078983>

848 Magny, M., Guiot, J., Schoellammer, P., 2001. Quantitative Reconstruction of Younger Dryas
849 to Mid-Holocene Paleoclimates at Le Locle, Swiss Jura, Using Pollen and Lake-Level Data.
850 *Quat. Res.* 56, 170–180. <https://doi.org/10.1006/qres.2001.2257>

851 Maisch, M., 1981. Glazialmorphologische und gletschergeschichtliche Untersuchungen im
852 Gebiet zwischen Landwasser- und Albulatal (Kt. Graubünden, Schweiz).

853 Marcott, S.A., Shakun, J.D., Clark, P.U., Mix, A.C., 2013. A Reconstruction of Regional and
854 Global Temperature for the Past 11,300 Years. *Science* 339, 1198–1201.
855 <https://doi.org/10.1126/science.1228026>

856 Martin, L.C.P., Blard, P.-H., Balco, G., Lavé, J., Delunel, R., Lifton, N., Laurent, V., 2017.
857 The CREp program and the ICE-D production rate calibration database: A fully
858 parameterizable and updated online tool to compute cosmic-ray exposure ages. *Quat.*
859 *Geochronol.* 38, 25–49. <https://doi.org/10.1016/j.quageo.2016.11.006>

860 Merchel, S., Arnold, M., Aumaître, G., Benedetti, L., Bourlès, D.L., Braucher, R., Alfimov,
861 V., Freeman, S.P.H.T., Steier, P., Wallner, A., 2008. Towards more precise ^{10}Be and ^{36}Cl
862 data from measurements at the 10–14 level: Influence of sample preparation. *Nucl. Instrum.*
863 *Methods Phys. Res. Sect. B Beam Interact. Mater. At.* 266, 4921–4926.
864 <https://doi.org/10.1016/j.nimb.2008.07.031>

865 Moran, A.P., Ivy-Ochs, S., Schuh, M., Christl, M., Kerschner, H., 2016. Evidence of central
866 Alpine glacier advances during the Younger Dryas–early Holocene transition period. *Boreas*
867 n/a-n/a. <https://doi.org/10.1111/bor.12170>

868 Oerlemans, J., 2005. Extracting a Climate Signal from 169 Glacier Records. *Science* 308,
869 675–677. <https://doi.org/10.1126/science.1107046>

870 Osmaston, H., 2005. Estimates of glacier equilibrium line altitudes by the Area×Altitude, the

871 Area×Altitude Balance Ratio and the Area×Altitude Balance Index methods and their
872 validation. *Quat. Int.* 138–139, 22–31. <https://doi.org/10.1016/j.quaint.2005.02.004>

873 Payot, V., 1884. Oscillations des quatre grands glaciers de la vallée de Chamonix et
874 énumération des ascensionnistes au Mont-Blanc. Sandoz, Genève.

875 Pellitero, R., Rea, B.R., Spagnolo, M., Bakke, J., Hughes, P., Ivy-Ochs, S., Lukas, S.,
876 Ribolini, A., 2015. A GIS tool for automatic calculation of glacier equilibrium-line altitudes.
877 *Comput. Geosci.* 82, 55–62. <https://doi.org/10.1016/j.cageo.2015.05.005>

878 Pellitero, R., Rea, B.R., Spagnolo, M., Bakke, J., Ivy-Ochs, S., Frew, C.R., Hughes, P.,
879 Ribolini, A., Lukas, S., Renssen, H., 2016. GlaRe, a GIS tool to reconstruct the 3D surface of
880 palaeoglaciers. *Comput. Geosci.* 94, 77–85. <https://doi.org/10.1016/j.cageo.2016.06.008>

881 Rabatel, A., Letréguilly, A., Dedieu, J.-P., Eckert, N., 2013. Changes in glacier equilibrium-
882 line altitude in the western Alps from 1984 to 2010: evaluation by remote sensing and
883 modeling of the morpho-topographic and climate controls. *The Cryosphere* 7, 1455–1471.
884 <https://doi.org/10.5194/tc-7-1455-2013>

885 Rabatel, A., Sanchez, O., Vincent, C., Six, D., 2018. Estimation of Glacier Thickness From
886 Surface Mass Balance and Ice Flow Velocities: A Case Study on Argentière Glacier, France.
887 *Front. Earth Sci.* 6. <https://doi.org/10.3389/feart.2018.00112>

888 Rea, B.R., 2009. Defining modern day Area-Altitude Balance Ratios (AABRs) and their use
889 in glacier-climate reconstructions. *Quat. Sci. Rev.* 28, 237–248.
890 <https://doi.org/10.1016/j.quascirev.2008.10.011>

891 Renssen, H., Goosse, H., Roche, D.M., Seppä, H., 2018. The global hydroclimate response
892 during the Younger Dryas event. *Quat. Sci. Rev.* 193, 84–97.
893 <https://doi.org/10.1016/j.quascirev.2018.05.033>

894 Réveillet, M., Vincent, C., Six, D., Rabatel, A., 2017. Which empirical model is best suited to
895 simulate glacier mass balances? *J. Glaciol.* 63, 39–54. <https://doi.org/10.1017/jog.2016.110>

896 Scherler, D., Bookhagen, B., Strecker, M.R., 2011. Spatially variable response of Himalayan
897 glaciers to climate change affected by debris cover. *Nat. Geosci.* 4, 156–159.
898 <https://doi.org/10.1038/ngeo1068>

899 Schimmelpfennig, I., Schaefer, J.M., Akçar, N., Koffman, T., Ivy-Ochs, S., Schwartz, R.,
900 Finkel, R.C., Zimmerman, S., Schlüchter, C., 2014. A chronology of Holocene and Little Ice
901 Age glacier culminations of the Steingletscher, Central Alps, Switzerland, based on high-
902 sensitivity beryllium-10 moraine dating. *Earth Planet. Sci. Lett.* 393, 220–230.
903 <https://doi.org/10.1016/j.epsl.2014.02.046>

904 Schindelwig, I., Akçar, N., Kubik, P.W., Schlüchter, C., 2012. Lateglacial and early Holocene

905 dynamics of adjacent valley glaciers in the Western Swiss Alps. *J. Quat. Sci.* 27, 114–124.
906 <https://doi.org/10.1002/jqs.1523>

907 Schwander, J., Eicher, U., Ammann, B., 2000. Oxygen isotopes of lake marl at Gerzensee and
908 Leysin (Switzerland), covering the Younger Dryas and two minor oscillations, and their
909 correlation to the GRIP ice core. *Palaeogeogr. Palaeoclimatol. Palaeoecol.* 159, 203–214.
910 [https://doi.org/10.1016/S0031-0182\(00\)00085-7](https://doi.org/10.1016/S0031-0182(00)00085-7)

911 Six, D., Vincent, C., 2014. Sensitivity of mass balance and equilibrium-line altitude to climate
912 change in the French Alps. *J. Glaciol.* 60, 867–878. <https://doi.org/10.3189/2014JoG14J014>

913 Smiraglia, C., Azzoni, R.S., D'Agata, C., Maragno, D., Fugazza, D., Diolaiuti, G.A., 2015.
914 The evolution of the Italian glaciers from the previous data base to the New Italian Inventory.
915 Preliminary considerations and results. *Geogr. Fis. E Din. Quat.* 38, 79–87.

916 Smiraglia, C., Diolaiuti, G., Casati, D., Kirkbride, M.P., 2010. Recent areal and altimetric
917 variations of Miage Glacier (Monte Bianco massif, Italian Alps) 264, 7.

918 Solomina, O.N., Bradley, R.S., Jomelli, V., Geirsdottir, A., Kaufman, D.S., Koch, J., McKay,
919 N.P., Masiokas, M., Miller, G., Nesje, A., Nicolussi, K., Owen, L.A., Putnam, A.E., Wanner,
920 H., Wiles, G., Yang, B., 2016. Glacier fluctuations during the past 2000 years. *Quat. Sci. Rev.*
921 149, 61–90. <https://doi.org/10.1016/j.quascirev.2016.04.008>

922 Vincent, C., Le Meur, E., Six, D., Funk, M., 2005. Solving the paradox of the end of the Little
923 Ice Age in the Alps. *Geophys. Res. Lett.* 32, L09706. <https://doi.org/10.1029/2005GL022552>

924 Vincent, C., Soruco, A., Six, D., Le Meur, E., 2009. Glacier thickening and decay analysis
925 from 50 years of glaciological observations performed on Glacier d'Argentière, Mont Blanc
926 area, France. *Ann. Glaciol.* 50, 73–79.

927 Wurth, G., Niggemann, S., Richter, D.K., Mangini, A., 2004. The Younger Dryas and
928 Holocene climate record of a stalagmite from Hölloch Cave (Bavarian Alps, Germany). *J.*
929 *Quat. Sci.* 19, 291–298. <https://doi.org/10.1002/jqs.837>

930 Young, N.E., Schaefer, J.M., Briner, J.P., Goehring, B.M., 2013. A ^{10}Be production-rate
931 calibration for the Arctic. *J. Quat. Sci.* 28, 515–526. <https://doi.org/10.1002/jqs.2642>

932